Cell Reports

Article

ARNT2 controls prefrontal somatostatin interneurons mediating affective empathy

Graphical abstract

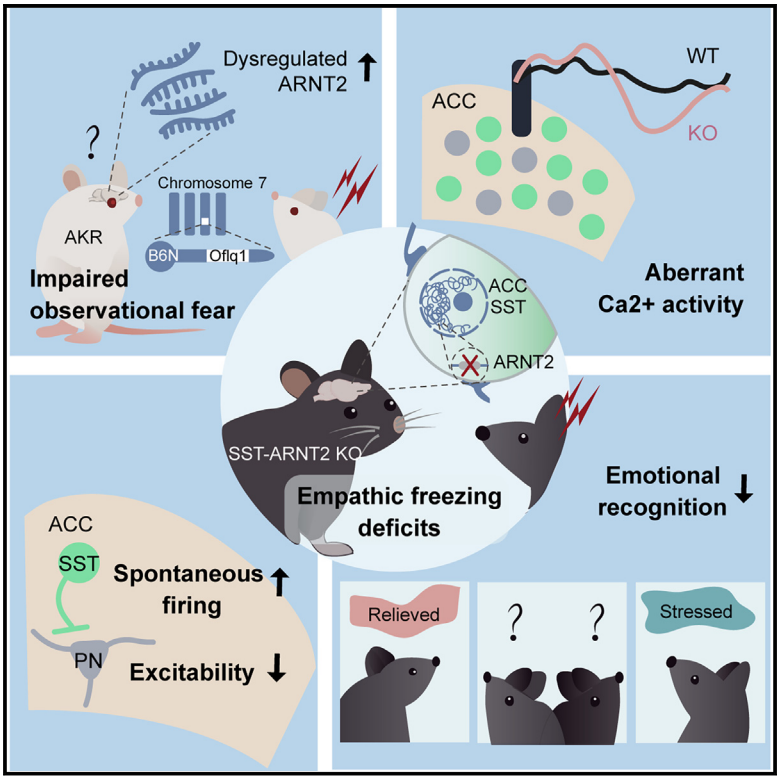

Highlights

- Forward genetic mapping in inbred mice identifies a locus (*Oflq1*) for observational fear
- Aberrant ARNT2 expression in the ACC reduces vicarious freezing behavior
- SST-ARNT2 KO mice exhibit altered spontaneous firing, calcium dynamics, and theta oscillations
- ARNT2-expressing SST neurons control empathic freezing and affective state discrimination

Authors

Jiye Choi, Seungmoon Jung, Jieun Kim, ..., Hee-Sup Shin, Sehyun Chae, Sehoon Keum

Correspondence

shchae@kangwon.ac.kr (S.C.), sdukeum@ibs.re.kr (S.K.)

In brief

Choi et al. demonstrate that altered expression of ARNT2 leads to deficits in observational fear and that ARNT2-expressing somatostatin (SST) interneurons in the anterior cingulate cortex (ACC) play a crucial role in regulating empathic freezing responses and the ability to discriminate emotional states in conspecifics.

Choi et al., 2024, Cell Reports *43*, 114659
September 24, 2024
https://doi.org/10.1016/j.celrep.2024.114659

CellPress

Cell Reports

CellPress
OPEN ACCESS

Article

ARNT2 controls prefrontal somatostatin interneurons mediating affective empathy

Jiye Choi,[1,8] Seungmoon Jung,[1,8] Jieun Kim,[2,3] Dahm So,[1,4] Arie Kim,[1] Sowon Kim,[1] Sungjoon Choi,[1] Eunsu Yoo,[1] Jee Yeon Kim,[1] Yoon Cheol Jang,[5] Hyoin Lee,[1] Jeongyeon Kim,[6] Hee-Sup Shin,[1] Sehyun Chae,[3,7,*] and Sehoon Keum[1,9,*]

[1]Center for Cognition and Sociality, Institute for Basic Science, Daejeon 34126, South Korea
[2]Department of Bio-Health Technology, College of Biomedicine Science, Kangwon National University, Chuncheon 24341, South Korea
[3]Multidimensional Genomics Research Center, Kangwon National University, Chuncheon 24341, South Korea
[4]Department of Bio and Brain Engineering, Korea Advanced Institute of Science and Technology, Daejeon 34141, South Korea
[5]Research Solution Center, Institute for Basic Science, Daejeon 34126, South Korea
[6]Emotion, Cognition and Behavior Research Group, Korea Brain Research Institute, Daegu 41062, South Korea
[7]Division of Chemical Engineering and Bioengineering, College of Art, Culture and Engineering, Kangwon National University, Chuncheon 24341, South Korea
[8]These authors contributed equally
[9]Lead contact
*Correspondence: shchae@kangwon.ac.kr (S.C.), sdukeum@ibs.re.kr (S.K.)
https://doi.org/10.1016/j.celrep.2024.114659

SUMMARY

Empathy, crucial for social interaction, is impaired across various neuropsychiatric conditions. However, the genetic and neural underpinnings of empathy variability remain elusive. By combining forward genetic mapping with transcriptome analysis, we discover that aryl hydrocarbon receptor nuclear translocator 2 (ARNT2) is a key driver modulating observational fear, a basic form of affective empathy. Disrupted ARNT2 expression in the anterior cingulate cortex (ACC) reduces affect sharing in mice. Specifically, selective ARNT2 ablation in somatostatin (SST)-expressing interneurons leads to decreased pyramidal cell excitability, increased spontaneous firing, aberrant Ca^{2+} dynamics, and disrupted theta oscillations in the ACC, resulting in reduced vicarious freezing. We further demonstrate that ARNT2-expressing SST interneurons govern affective state discrimination, uncovering a potential mechanism by which *ARNT2* polymorphisms associate with emotion recognition in humans. Our findings advance our understanding of the molecular mechanism controlling empathic capacity and highlight the neural substrates underlying social affective dysfunctions in psychiatric disorders.

INTRODUCTION

Empathy, the ability to recognize and understand the affective states of others, is fundamental for our social interactions and mental well-being.[1,2] Empathic abilities exhibit significant individual variations.[3–5] Moreover, disturbances in empathy, including an inability to accurately detect emotions in others, are prominent features of a number of neuropsychiatric conditions, such as autism, anti-social personality disorder, schizophrenia, alexithymia, and psychopathy.[6–9] Previous candidate gene studies have highlighted the role of various neurochemicals—including oxytocin, vasopressin, dopamine, serotonin, and opioids—and genetic variations in their receptor genes in the formation and modulation of empathy-related behaviors.[10–15] Recent genome-wide association studies revealed several genetic factors significantly associated with empathic traits.[5,16] However, despite these findings, the gene variants proposed to contribute to individual variability in empathy have not been consistently replicated across different human studies,[17,18] possibly due to genetic heterogeneity and uncontrolled environmental variables. Furthermore, the underlying neurobiological mechanisms are yet to be determined.

Observational fear is a basic form of affective empathy whereby an observer witnesses a demonstrator receiving aversive stimuli, such as foot shocks, and responds with fear.[19,20] This socially evoked vicarious freezing response, referred to as emotional state matching or affect sharing, is considered a measure of empathy-like traits in rodents.[21–23] Converging evidence suggests that the functional organization of observational fear circuits in rodents is similar to the core neural networks involved in empathy for pain or distress in humans.[24] In particular, the anterior cingulate cortex (ACC), a node central to encoding affective and cognitive information in empathy, is required for acquisition of observational fear in mice.[19,24,25] While significant progress has been made in understanding the executive neural circuit of observational fear,[26–30] the specific genes and underlying neurobiological mechanisms at synaptic and molecular levels remain poorly understood. Interestingly, vicarious freezing varies considerably among different inbred mouse strains, indicating genetic control of innate empathic fear responses.[31] In

this study, we found that the AKR/J (AKR) strain of mice exhibits blunted affect sharing, which is not attributable to abnormalities in sensory perception, anxiety, or social interaction. To identify a specific gene that is critical to variations in vicarious freezing, we employed a forward genetic approach, mapping a single quantitative trait locus (QTL) for observational fear. Through RNA sequencing (RNA-seq) and loss-of-function studies, we identified that the *Arnt2* gene encoding a basic-helix-loop-helix (bHLH)-Per-Arnt-Sim (PAS) family transcription factor is essential for the acquisition of observational fear. Subsequent cellular, electrophysiological, *in vivo* Ca^{2+} imaging, and local field potential (LFP) recording experiments collectively demonstrated that ARNT2 is necessary for the activities of somatostatin (SST) interneurons in the ACC that mediate vicarious freezing response. Given the genetic association between *ARNT2* polymorphism and emotion recognition in humans,[32] we further demonstrated that ARNT2 plays a crucial role in affective state discrimination in mice. Our study provides valuable insights into the molecular mechanisms underlying the affective capacity of empathy behaviors.

RESULTS

Identification of a genetic locus (QTL) that determines observational fear

We first sought to establish robust differences in observational fear learning (Figure 1A) between two inbred mouse strains to use as a platform for uncovering observational fear-specific genetic factors. Mice of the AKR inbred strain exhibited a significantly reduced observational fear learning compared with B6N mice (Figures 1B and 1C). Previous studies have reported that AKR mice exhibit visual acuity and auditory brainstem responses comparable to those of B6N mice, which possess good vision and hearing abilities.[33–36] Our findings revealed that the AKR strain exhibited a lower level of center time compared to B6N mice in the open field task (Figures S1A and S1B). However, the center time of AKR mice appears similar to that of multiple other inbred strains that exhibit relatively higher levels of observational freezing, as reported in our previous study.[31] Additionally, no significant difference was found in the time spent on the open arms in the elevated plus maze between AKR and B6N strains (Figure S1C). Collectively, these findings suggest that the diminished observational fear response in the AKR strain is unlikely to be attributable to an anxiety-like trait. Furthermore, we found no significant difference in locomotion, conditioned fear, or sociability between these two strains (Figures S1D–S1F).

During observational fear conditioning (OFC), the demonstrator mice display various sensory and emotional reactions to foot shocks, including jumping, running, distress vocalization, and freezing. These behaviors serve as social cues, triggering vicarious freezing (emotional contagion) in the observer mice. Accordingly, it is possible that the low freezing response observed in AKR observer mice could be due to differences in the display of visual, olfactory, or auditory social cues by AKR demonstrator mice while receiving foot shocks.[19,31] To examine whether the observers' freezing response differs between in-group and out-group demonstrators, we assessed observational fear in AKR mice paired with B6N demonstrators (Figure S2A). Intriguingly, despite the different responses to foot shocks between B6N and AKR demonstrators (Figure S2B), AKR observers showed similar deficits in vicarious freezing behavior when paired with out-group B6N demonstrators as they did with in-group AKR demonstrators (Figure S2C). Furthermore, while AKR observers exhibited lower levels of gazing responses compared to B6N mice (Figure S2D), we found no significant correlation between gazing behavior and vicarious freezing response in either strain (Figures S2E and S2F). These findings suggest that although distress cues manifested by demonstrators may vary across mouse strains, such strain-specific differences are unlikely to be the primary factors contributing to the reduced vicarious freezing behavior in AKR observer mice. Based on these results, we hypothesize that the deficits in observational fear in AKR observer mice are due to genetic variations specifically affecting their capacity to respond to demonstrators' distress, rather than from sensory abnormalities.

To identify a causative variant, a forward genetic mapping analysis was employed in an F2 population of 190 male mice (derived from a reciprocal F1 intercross of B6N and AKR hybrids) in which each individual mouse carried a unique combination of B6N and AKR gene variants (Figure 1D). The phenotypic variation in vicarious freezing in F2 progeny greatly exceeded that of the AKR and B6N inbred strains (Figure 1E), suggesting the contribution of multiple genetic loci. All mice were subsequently genotyped for 197 single-nucleotide polymorphism (SNP) markers that were informative in this cross. We identified a single QTL, *Oflq1* (observational fear learning QTL1) on chromosome 7 that was significant at a genome-wide p value of <0.01 (LOD [logarithm of the odds] score = 11.9) (Figures 1F and S3A). *Oflq1* accounted for 23% of the phenotypic variance in observational fear responses in the F2 population. To determine the allelic contribution of the effect of *Oflq1*, we evaluated vicarious freezing responses of 190 F2 mice against the genotype of the peak SNP marker, rs13479392, at the highest LOD score. Observational fear incrementally decreased in F2 animals homozygous for the AKR allele at rs13479392 compared with that of F2 mice heterozygous or homozygous for the B6N allele (Figure S3B). Notably, *Oflq1* was also detected in the 24-h memory retrieval (LOD score = 9.0) (Figures S3C and S3D). Not surprisingly, there was a positive correlation between acquisition and retrieval of observational fear (Figure S3E), suggesting that variations in 24-h contextual memory in the F2 population result from differences in the level of vicarious fear expression on day 1.

Next, to validate the phenotypic effects of the isolated *Oflq1*, we generated a congenic mouse line by breeding AKR mice with B6N mice through marker-assisted backcrossing for ten generations (Figure 1G). We attempted to create congenic mice harboring the AKR *Oflq1* genomic segment on the B6N genetic background, based on the hypothesis that this region of the AKR genome could lead to deficits in observational fear. Ultimately, we established a recombinant congenic mouse, B6N.AKR-*Oflq1*, carrying homozygous alleles from the AKR *Oflq1* segment spanning 83.5–91.2 Mbp on chromosome 7. Compared to control B6N animals, these congenic mice exhibited significantly decreased observational fear behaviors (Figures 1G–1I). This result identifies the 83.5-Mbp (rs36537392) to 91.2-Mbp (D7Mit301) interval as the critical

CellPress
OPEN ACCESS

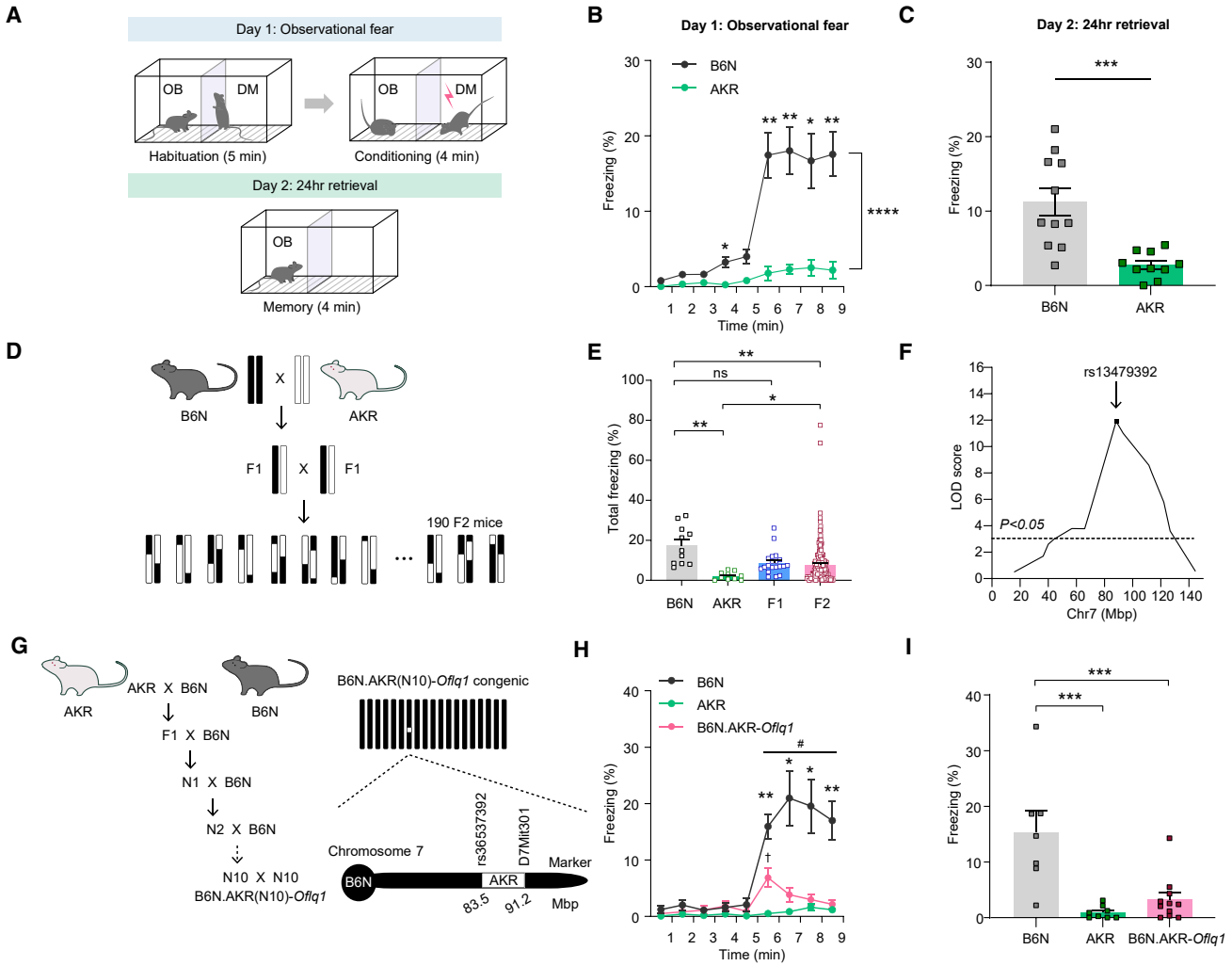

Figure 1. Identification of the *Oflq1* that determines observational fear

(A) Diagram of observational fear chamber and outline of behavioral paradigm. Day 1: observational fear conditioning. Observer (OB) and demonstrator (DM) mice are individually placed in the chamber and allowed to explore for 5 min (habituation). The OB mouse then witnesses a DM mouse receiving foot shocks through a transparent partition for 4 min (conditioning). Day 2: 24-h retrieval. The OB mouse is returned alone to the same chamber in the absence of a DM mouse and shocks.

(B and C) Vicarious freezing of B6N (black) and AKR (green) OB mice were measured on day 1 (B), followed subsequently by measurement of 24-h contextual memory (C). AKR mice showed a significantly reduced observational fear response and 24-h memory compared with B6N mice.

(D) Breeding strategy. 190 F2 progeny were generated by a reciprocal intercross of F1 (B6N × AKR) mice.

(E) Total freezing (%) during the 4-min conditioning period of OFC in four inbred strains of mice. The level of vicarious freezing in 190 F2 mice was significantly different from that in the two parental B6N or AKR strains.

(F) A single genome-wide significant QTL for vicarious freezing response was identified on chromosome 7 that peaked at the SNP marker (rs13479392) (LOD score = 11.9).

(G) A breeding strategy to generate a congenic mouse strain that carries a segment of AKR chromosome 7 spanning from 83.5 Mbp (rs36537392) to 91.2 Mbp (D7Mit301) introgressed into the B6N background. The black color represents the B6N origin, while white indicates the AKR origin.

(H and I) B6N.AKR-*Oflq1* congenic mice carrying the AKR *Oflq1* segment (83.5–91.2 Mbp) exhibit a significant difference in both observational fear and 24-h memory compared to B6N and AKR mice.

Error bars represent SEM. $^{*,\#,\dagger}p < 0.05$, $^{**}p < 0.01$, $^{***}p < 0.001$ by two-way repeated-measures (RM) ANOVA followed by Šídák's post hoc test (B and H), Mann-Whitney two-tailed t test (C), and Kruskal-Wallis one-way ANOVA on ranks by Dunn's test (E and I). In this and in all subsequent figures, bars without asterisks did not reach significance (ns, $p > 0.05$). ANOVAs, *F* values, *t* values, and all additional statistical information for this and subsequent figures can be found in Table S1. See also Table S1; Figures S1–S3.

region harboring the *Oflq1* locus (Figure 1G). We found no significant difference in classical fear conditioning between B6N.AKR-*Oflq1* congenic and B6N mice (Figure S3F), indicating that the reduced vicarious freezing in congenic mice is not attributable to diminished acquisition of conditioned fear. Taken together, these results demonstrate that a causal gene(s)

within the *Oflq1* locus is sufficient and selective in driving variations in observational fear. Intriguingly, B6N.AKR-*Oflq1* congenic mice exhibited a higher vicarious freezing response compared with AKR mice (Figure 1H), suggesting that the decreased observational fear response in the AKR strain may not be predominantly attributable to the effects of a single *Oflq1* locus. The behavioral differences observed between the AKR and B6N strains may be influenced by the phenotypic effects of multiple other minor genetic loci (Figure S3A).

Dysregulated ARNT2 expression reduces observational fear

The congenic line (B6N.AKR-*Oflq1*) significantly narrowed the *Oflq1* critical interval that determines the level of vicarious freezing to 7.7 Mbp (Figure 1G), but this region harbors 65 annotated protein-coding genes and 27 non-coding RNAs (Table S2).[37] Thus, we next aimed to identify the gene(s) within the *Oflq1* locus that is causally implicated in driving variation in observational fear. To systematically examine the molecular changes that account for the differences between AKR and B6N mice, we performed RNA-seq gene-expression profiling of the ACC in both naive and post-OFC states (Figure 2A). We then compared gene-expression profiles, selecting a total of 1,779 differentially expressed genes (DEGs) between the two mouse strains, including 1,453 DEGs for the naive state and 921 DEGs for the post-OFC (Figures 2B and 2C; Table S3). Among DEGs, 595 were shared between naive and post-observational fear conditions (Figure 2D). Collectively, these data indicate a significant difference in gene-expression patterns in the ACC between AKR and B6N mice. Of the genes located within the 7.7-Mbp *Oflq1* congenic interval, *Arnt2*, *Fah*, *Me3*, and *Sytl2* were upregulated in naive AKR mice compared with naive B6N mice, whereas *Cemip* and *Prss23* were downregulated (Figures 2E and S4). Remarkably, among the genes within this interval, only *Arnt2* (aryl hydrocarbon receptor nuclear translocator 2) exhibited altered expression following OFC, suggesting its differential recruitment before and after the behavior (Figures 2C and 2E). We subsequently confirmed the elevated mRNA and protein levels of *Arnt2* in AKR mice compared to the B6N strain (Figures 2F and 2G). Additionally, the AKR allele of the *Arnt2* transcript in B6N.AKR-*Oflq1* congenic mice exhibited a significantly higher level than that in control B6N mice, consistent with levels seen in AKR mice. This finding further supports the role of *cis*-regulatory genetic variation in determining *Arnt2* mRNA abundance in the ACC of AKR mice. Given its differential expression in the ACC between the two parental strains in both naive and post-OFC states, as well as its implications in activity-dependent neuronal gene expression,[38,39] *Arnt2* emerged as the most promising candidate gene for further investigation of its role in observational fear.

To determine whether ARNT2 could causally drive changes in observational fear, we designed and injected an adeno-associated virus (AAV) expressing a small hairpin (interfering) RNA (shRNA) construct targeting *Arnt2* into the right hemisphere of the ACC and then performed behavioral testing (Figure 3A). Notably, we chose to knock down *Arnt2* in the ACC of the AKR strain due to the significantly higher level of ARNT2 in this strain compared with that in B6N mice. Given that ARNT2 regulates activity-dependent neural gene expression,[38,39] we expected that this manipulation could significantly contribute to alterations in observational fear. Indeed, diminished expression of ARNT2 in the AAV-infected ACC of AKR mice significantly enhanced the level of vicarious freezing compared with that in AKR mice expressing non-targeting control shRNA (Figures 3B and 3C). To further confirm that the elevated expression of ARNT2 causes deficits in observational fear, we injected the same AAV expressing an *Arnt2* shRNA into the ACC of B6N.AKR-*Oflq1* congenic mice. Indeed, the vicarious freezing response was significantly increased in congenic mice that received the *Arnt2*-knockdown virus as compared with control virus-injected mice (Figure 3D). Thus, these results indicate a causal relation between elevated expression of ARNT2, specifically in the ACC, and disrupted observational fear in AKR mice.

ARNT2 deficiency in SST neurons in the ACC reduces observational fear

To further substantiate our findings, we sought to induce transcriptional activation of the *Arnt2* gene within its endogenous genomic locus using an AAV-based synergistic activation mediator system.[40] This system comprises three components: an *Arnt2*-specific guide RNA (gRNA), an MS2/P65/HSF1 transcription activation complex, and a catalytically inactive Cas9 (dCas9) fused to the VP64 transcriptional activator (Figure S5A).[41] We expected that increasing ARNT2 expression would decrease observational fear response. Compared to the control condition using dCas9/VP64 with a scrambled gRNA, we observed a significant increase in *Arnt2* mRNA levels (1.4-fold) in the ACC region injected with AAVs carrying dCas9/VP64 and *Arnt2*-targeting gRNA (Figure S5B). However, this CRISPR-mediated transcriptional activation of the *Arnt2* gene in the ACC did not lead to changes in observational fear response (Figure S5C). We next determined whether the knockdown of *Arnt2* had any demonstrable effect in B6N mice. We injected the AAV expressing sh*Arnt2* into the ACC of B6N mice, with the expectation that reducing ARNT2 expression would further increase observational fear. Surprisingly, B6N mice injected with the sh*Arnt2* virus exhibited a significantly decreased observational fear response compared with B6N mice injected with the control virus (Figure 3E). A previous study demonstrated that ARNT2 has distinct dual functions in regulating neuronal gene expression.[38] By recruiting different cofactors in basal and stimulated states, ARNT2 exerts contradictory effects on activity-regulated transcription, thereby maintaining an appropriate level of somatic inhibition.

The role of ARNT2 has never been defined in different cell types or explored in any behaviors. Homozygous *Arnt2*-null mutant mice die perinatally due to impaired hypothalamic development.[42,43] Thus, to elucidate the mechanistic role of ARNT2 in the function of the ACC, we generated a conditional allele of the *Arnt2* gene and employed cell-type-specific knockout (KO) mice (Figures 4A–4C). First, to selectively delete *Arnt2* in excitatory glutamatergic neurons of the brain, we generated Vglut2-ARNT2 KO ($Vglut2^{Cre/+}$;$Arnt2^{F/F}$) mice by breeding $Arnt2^{F/F}$ mice with Vglut2 (vesicular-glutamate transporter 2, also known as *Slc17a6*)-Cre mice. However, in line with the perinatal lethality observed in homozygous *Arnt2*-null mutant mice,[42,43]

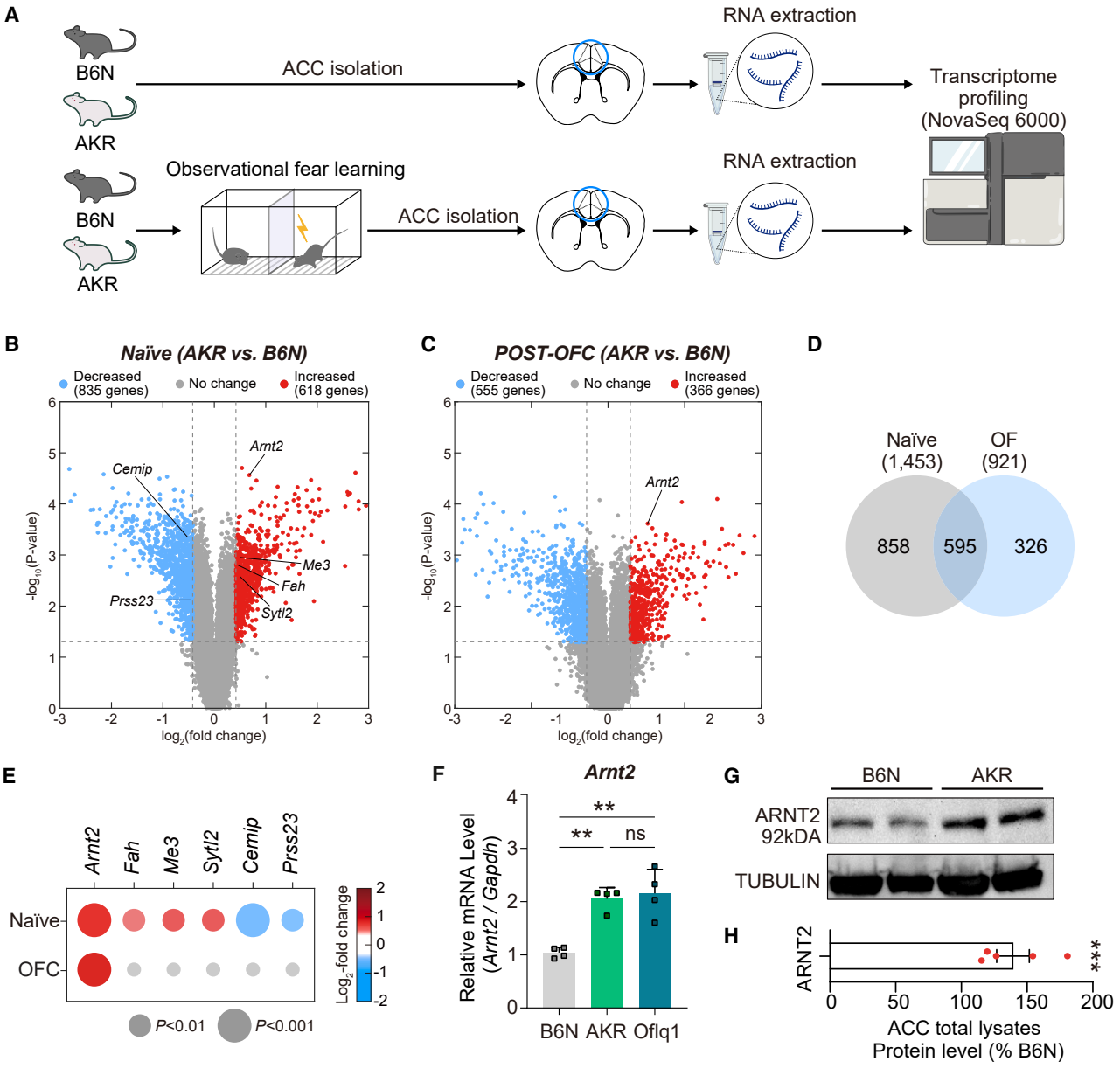

Figure 2. Gene-expression profiling analysis of the ACC in AKR and B6N mice under naive and post-observational fear-conditioning states

(A) Workflow of sample preparation and RNA sequencing.

(B and C) Volcano plots for (B) naive and (C) post-observational fear-conditioning states show differentially expressed genes (DEGs) in AKR mice compared to B6N mice. Red and blue dots represent upregulated and downregulated genes, respectively; gray dots represent genes whose expressions were not significantly different.

(D) Comparison of DEGs in the ACC between naive and post-observational fear-conditioning states. The total number of DEGs in each comparison is indicated in parentheses.

(E) DEGs located within the *Oflq1* congenic interval. The color bar represents the gradient of $\log_2$ fold changes, indicating the degree of upregulation or downregulation.

(F) Quantitative real-time PCR analysis showed higher expression levels of the AKR allele for *Arnt2* mRNA transcript in the ACC of naive AKR mice compared with the naive B6N strain. The averages from three independent experiments are shown.

(G and H) Western blot analyses of ACC lysates demonstrated that the abundance of ARNT2 protein was higher in naive AKR mice than in the B6N strain (P70).

(H) ARNT2 protein level (%) in total ACC lysates of AKR mice compared to that in B6N mice.

Error bars represent SEM. $^{*}p < 0.05$, $^{**}p < 0.01$, $^{***}p < 0.001$ by Student's t test (F) and one-sample t test (H).

See also Table S1; Figure S4.

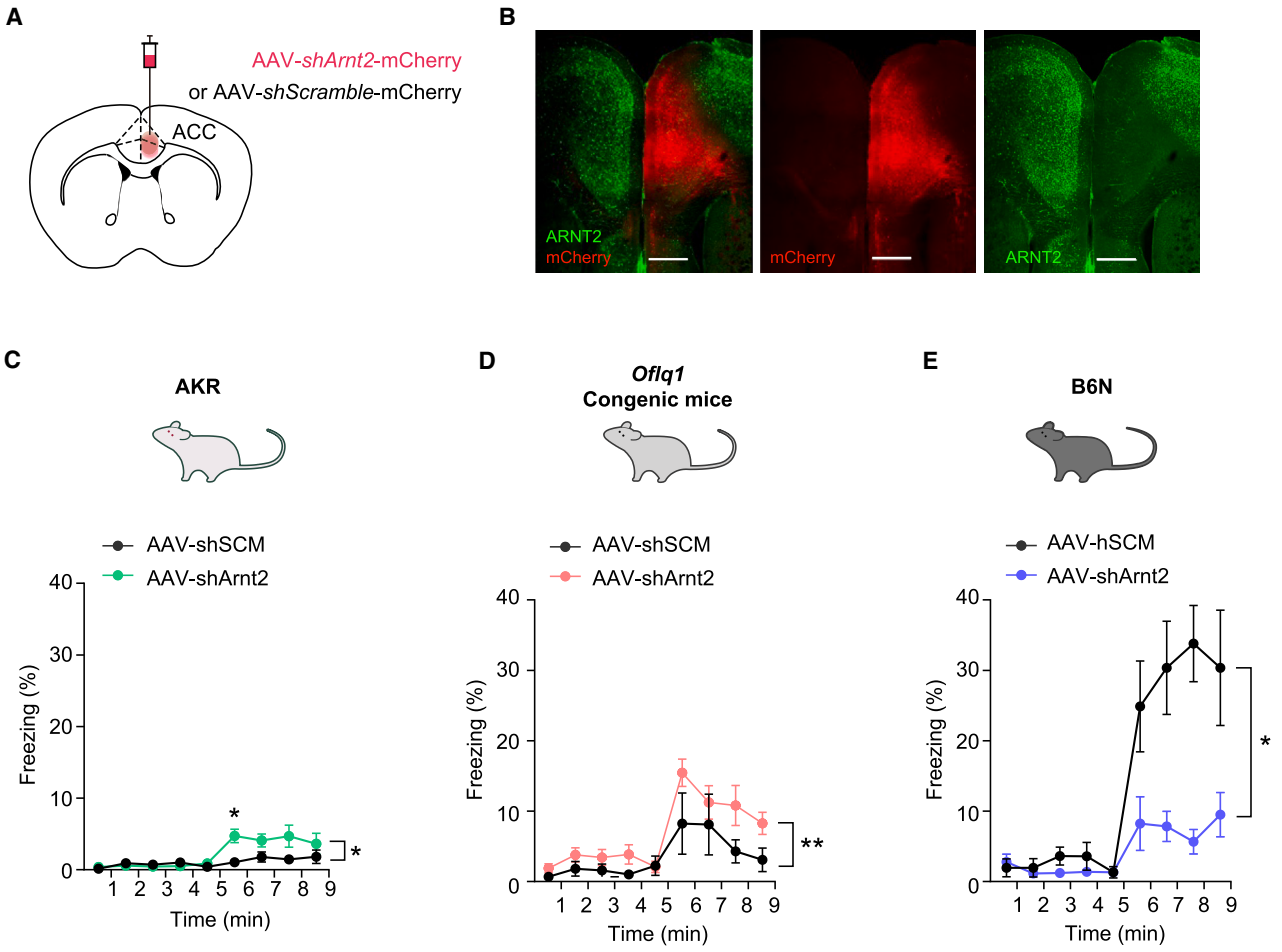

Figure 3. Dysregulated expression of ARNT2 in the ACC reduces observational fear

(A) Schematic of ARNT2 depletion by injection of AAV-U6-*shArnt2*-mCherry or AAV-U6-*shScramble*-mCherry into the right ACC.

(B) Representative confocal images of ARNT2 immunostaining in prefrontal cortex slices from AKR mouse with the ACC injection of AAV-U6-*shArnt2*-mCherry or AAV-U6-*shScramble*-(SCM)-mCherry (red, mCherry; green, ARNT2). Scale bars, 500 μm.

(C) Diminished expression of ARNT2 in the ACC of AKR mice increased observational fear.

(D) B6N.AKR-*Oflq1* congenic mice with shRNA-mediated knockdown of *Arnt2* expression showed significantly higher responses in observational fear compared with congenic mice that were injected with a scrambled control virus.

(E) Depletion of ARNT2 expression in the ACC of B6N mice reduced vicarious freezing response.

Data are presented as mean ± SEM. $^{*}p < 0.05$, $^{**}p < 0.01$, $^{***}p < 0.001$ by two-way RM ANOVA followed by Šídák's post hoc test (C–E).

See also Figure S5 and Table S1.

Vglut2-ARNT2 KO mice were not viable when bred to homozygosity (0 homozygous KO vs. 20 wild-type [WT] and 47 heterozygous live births). Heterozygous Vglut2-ARNT2 KO mice were viable, with no significant developmental defects; they displayed levels of observational fear similar to those of their WT littermates (Figure S6A). Accordingly, to confirm the impact of *Arnt2* deletion in pyramidal neurons of the ACC, we focally injected an AAV expressing Cre-recombinase under the control of the Ca^{2+}/calmodulin-dependent protein kinase IIα promoter (AAV-CamKIIα-Cre-GFP) into the ACC of *Arnt2*$^{F/F}$ mice. Quantification of ARNT2^{+}CAMK2A^{+} cells in the ACC revealed significant abrogation of ARNT2 in pyramidal neurons (Figure S6B). Observer mice with localized *Arnt2* deletion in ACC pyramidal neurons exhibited no difference in vicarious freezing response compared with control mice (Figure S6C). These results indicate that ARNT2 in ACC excitatory neurons is not critically involved in the regulation of observational fear.

Arnt2 is highly expressed in GABAergic inhibitory neurons in the cortex (http://dropviz.org).[38,44] To examine the role of ARNT2 in inhibitory neurons, we generated four lines of KO mice lacking ARNT2 in parvalbumin (PV)-expressing neurons (PV-ARNT2 KO), SST-expressing neurons (SST-ARNT2 KO), vasoactive intestinal peptide (VIP)-expressing neurons (VIP-ARNT2 KO), or neuron-derived neurotrophic factor (NDNF)-expressing neurons (NDNF-ARNT2 KO) by crossing *Arnt2*$^{F/F}$ mice with PV-Cre, SST-Cre, VIP-Cre, or NDNF-Cre mice, respectively. Collectively, these cell types represent the vast majority (>90%) of the GABAergic neuronal population in the cortex (Figure 4A).[45]

CellPress
OPEN ACCESS

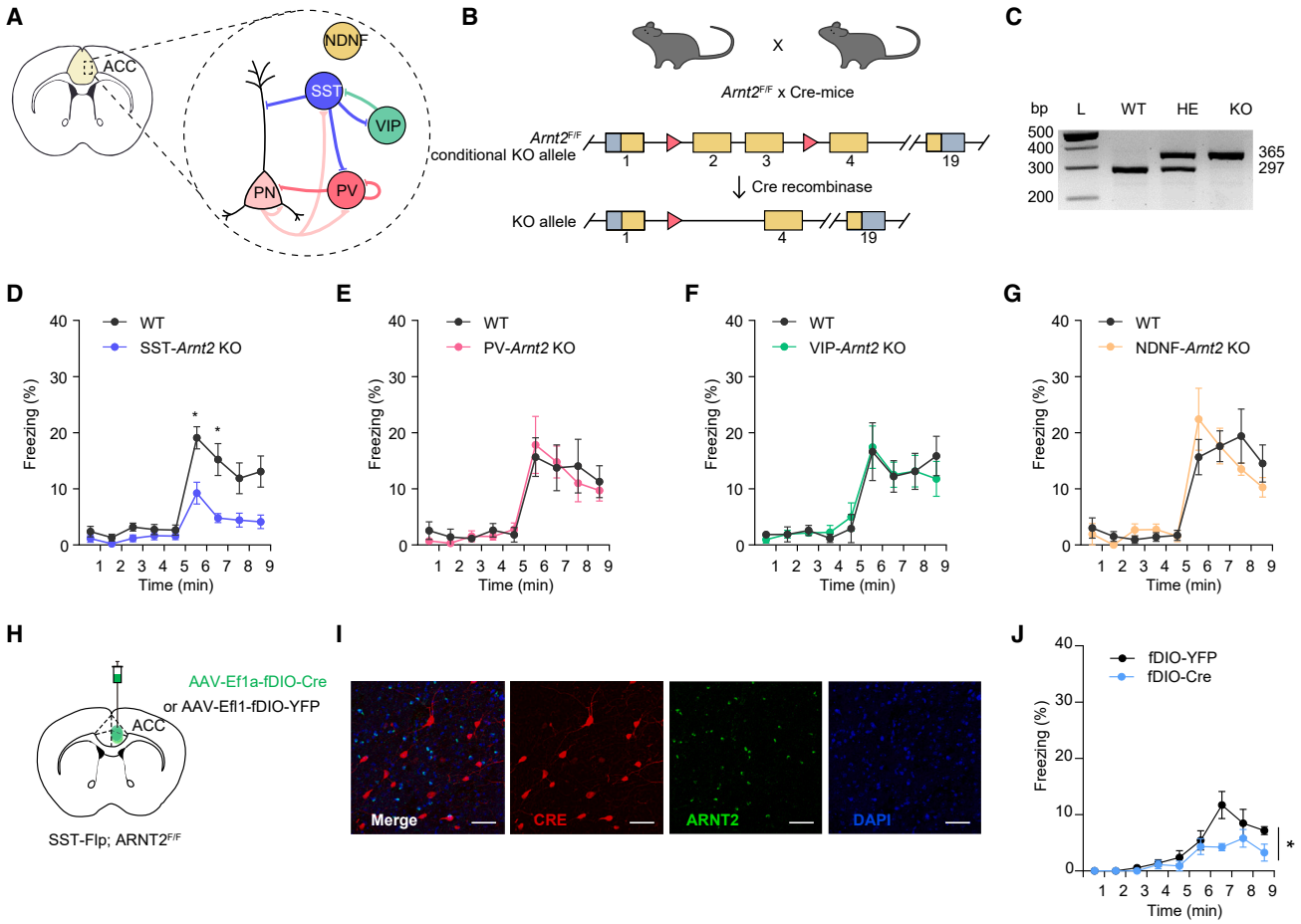

Figure 4. Loss of ARNT2 in SST neurons decreases observational fear response

(A) Schematic overview of the major neuronal populations of the microcircuit in the ACC. Pink triangle, pyramidal neuron (PN); red circle, PV interneuron; blue circle, SST interneuron; green circle, VIP interneuron; yellow circle, NDNF interneuron.

(B) Conditional targeting scheme of the *Arnt2* gene. A pair of *LoxP* (triangle, red) sites flanking exon 2-exon 3 of the *Arnt2* gene was knocked out in a cell-type-specific manner by Cre-recombinase.

(C) A PCR image showing the genotyping of conditional alleles of the *Arnt2* gene (WT, 297 bp; targeted, 365 bp). Wild-type (WT) mouse, $SST^{+/+}$;$Arnt2^{F/F}$; heterozygous (HET) mouse, $SST^{Cre/+}$;$Arnt2^{F/+}$; homozygous knockout (KO) mouse, $SST^{Cre/+}$;$Arnt2^{F/F}$.

(D) Deletion of *Arnt2* in SST neurons significantly reduced vicarious freezing behaviors compared to WT littermate controls.

(E) PV-ARNT2 KO mice showed no difference in observational fear compared to WT littermate controls.

(F) Vicarious freezing response was found to be similar in VIP-ARNT2 KO mice and WT littermate controls.

(G) There was no difference in observational fear between NDNF-ARNT2 KO mice and their WT littermate controls.

(H) Unilateral injection of AAV-fDIO-Cre to selectively delete ARNT2 in SST^{+} neurons in the ACC of an SST-Flp;$ARNT2^{F/F}$ mouse.

(I) A representative confocal image (image on left panel: blue, DAPI; green, ARNT2; red, CRE). Immunohistochemistry staining confirms the selective KO of ARNT2 in CRE (red)-expressing SST neurons, but not in CRE-negative neurons. Bregma 1.0 mm rostral. Scale bars, 50 μm.

(J) Mice with SST-specific ARNT2 deletion showed significantly reduced observational fear response.

Data are presented as mean ± SEM. $^{*}p < 0.05$, $^{**}p < 0.01$, $^{***}p < 0.001$ by two-way RM ANOVA followed by Šídák's post hoc test (D–G and J).

See also Figure S6 and Table S1.

Notably, SST-ARNT2 KO observer mice exhibited significantly reduced vicarious freezing behavior compared with their WT littermates (Figure 4D). By contrast, PV-ARNT2 KO, VIP-ARNT2 KO, and NDNF-ARNT2 KO mice showed no difference in observational fear compared with their respective WT controls (Figures 4E–4G). To further examine whether the diminished observational fear response in SST-ARNT2 KO mice is specifically due to the loss of ARNT2 in SST neurons in the ACC, we bred $SST^{Flp/+}$;$Arnt2^{F/F}$ mice, in which flippase (Flp) recombinase was selectively expressed in SST neurons in an $Arnt2^{F/F}$ background. We injected the ACC of these mice with an AAV driving Flp-dependent Cre-recombinase expression (AAV-fDIO-Cre; Figure 4H), enabling SST neuron-specific deletion of ARNT2 restricted to the ACC region (Figure 4I). Indeed, we found that this ACC-specific ablation of ARNT2 in SST neurons resulted in a reduced observational fear response (Figure 4J), phenocopying the deficit observed in SST-ARNT2 KO mice. Thus, the lack of ARNT2 specifically in SST neurons of the ACC is sufficient

to cause a reduction in observational fear response. We found no behavioral difference in classical fear conditioning between SST-ARNT2 KO and WT mice (Figure S6D), suggesting that selective ablation of ARNT2 in SST neurons reduces observational fear without affecting the acquisition of conditioned fear. Taken together, these findings indicate that SST-ARNT2 KO mice display behavioral deficits similar to those observed in B6N mice injected with the sh*Arnt2* knockdown virus in the ACC, supporting a specific role of ARNT2 in SST interneurons in the ACC in modulating observational fear.

Empathic freezing deficits from ACC dysfunction unrelated to conditioned fear

Observers with prior shock experiences demonstrate augmented vicarious freezing when witnessing similar aversive stimuli in others.[26,46–48] Notably, while the AKR strain, *Oflq1* congenic mice, and SST-ARNT2 KO mice showed reduced vicarious freezing responses, their conditioned fear responses were comparable to those of their respective WT controls (Figures S1D, S3F, and S6D). To elucidate whether the decreased observational fear response exhibited by these mouse strains originates from compromised ability to express empathic freezing rather than alterations in their fear responses, we investigated the effect of prior shock experience on subsequent observational fear (Figure S7A). We found that a single priming foot shock significantly augmented vicarious freezing in these strains compared to their naive control groups. Intriguingly, the freezing levels of shock-experienced AKR and *Oflq1* congenic mice were similar to those of naive B6N mice (Figure S7B). Moreover, prior shock exposure substantially increased the observational fear response in SST-ARNT2 KO mice, such that their freezing behavior did not significantly differ from shock-experienced WT littermate controls (Figure S7C).

Distinct neural mechanisms underlie observational freezing in naive versus shock-experienced observers.[24,49] Specifically, the OFC paradigm with naive observers exclusively measures empathic fear responses to foot shocks experienced by demonstrators.[19] Conversely, the OFC task with previously shocked observers predominantly assesses adaptive learned fear responses that are potentiated by socially triggered aversive memory.[29,47] The ACC is not essential for mediating the acquisition of observational fear in shock-experienced observers. Instead, hippocampal-amygdala fear-conditioning circuits are critical mediators of observational freezing in these experienced observers.[29] Thus, our findings demonstrate that while AKR and SST-ARNT2 KO mice can acquire contextual fear through observational learning, they exhibit a specific reduction in empathic freezing. This reduction is attributable to ACC dysfunction rather than alterations in conditioned fear circuits.

Dysregulated spontaneous firing, Ca^{2+} dynamics, and theta oscillation in SST-ARNT2 KO mice

SST interneurons primarily target distal dendrites of pyramidal cells, where they gate dendritic excitability, local dendritic and spine plasticity, and pyramidal neuron recruitment.[50,51] To investigate the functional impact of selectively deleting *Arnt2* in SST neurons, we performed whole-cell patch-clamp recordings in the right ACC in acute brain slices. To identify SST neurons, we crossed SST-ARNT2 KO mice with a Cre-dependent Rosa26LSL-tdTomato (Ai14) reporter line (*SST*$^{Cre/+}$;*Arnt2*$^{F/F}$;*Ai14*$^{F/+}$), which labels SST neurons with a red fluorescent protein. We first measured the intrinsic excitability of SST interneurons and putative pyramidal neurons in SST-ARNT2 KO mice. All recorded SST neurons lacking ARNT2 displayed no difference in firing discharge pattern and average frequency of action potential (Figures 5A and 5B). By contrast, pyramidal cells from SST-ARNT2 KO mice exhibited a significant decrease in firing frequency compared with those from WT animals, especially at high current intensities (Figures 5D and 5E). This decrease in firing rate was accompanied by a significant increase in the input resistance of pyramidal neurons in KO mice (Figure S8M). Both pyramidal cells and SST interneurons in SST-ARNT2 KO mice showed no difference in their action potential and intrinsic passive properties except input resistance of pyramidal neurons (Figure S8). To determine whether the observed change in excitability is affected by altered synaptic inputs, we monitored spontaneous firing activities of pyramidal neurons and SST interneurons in the ACC. Notably, loss of ARNT2 resulted in a significant increase in spontaneous firing rate of SST neurons (Figure 5C). Pyramidal neurons exhibited no difference in spontaneous firing, but the proportion of the spontaneously firing pyramidal cells decreased significantly in SST-ARNT2 KO mice (Figure 5F).

Next, to investigate how ARNT2 regulates the activity of SST neurons *in vivo* during observational fear, we measured the real-time Ca^{2+} dynamics of SST neurons in freely behaving animals using a fiber photometry system. Employing a viral strategy, we specifically expressed the genetically encoded Ca^{2+} indicator, GCaMP8f, in SST neurons and implanted an optical fiber to record Ca^{2+} transients as a proxy for population activity in WT (SST-Cre) and SST-ARNT2 KO mice (Figure 5G). Intriguingly, despite the varying durations of freezing in each event, the activity of SST neurons consistently decreased at the onset of vicarious freezing (Figures 5H and 5I). Notably, the Ca^{2+} signals of ARNT2-deficient SST neurons specific to vicarious freezing epochs were not only more robustly suppressed but also exhibited significant altered Ca^{2+} dynamics compared to WT SST neurons, with differences emerging prior to the onset of freezing (Figures 5H and 5J). The Ca^{2+} dynamics during the habituation immobility were not significantly different between WT and SST-ARNT2 KO mice (Figures S9A–S9C). Additionally, SST neuron activity in SST-ARNT2 KO mice did not differ from that of WT mice during demonstrators' pain responses or freezing epochs in the conditioning period (Figures S9D–S9I). During observational fear, rhythmic oscillations at the theta frequency are observed in the ACC and the basolateral amygdala (BLA).[19] To examine how aberrant activities of ARNT2-deficient SST neurons impact ACC functions, we recorded theta oscillations in the right ACC and BLA during freezing epochs of the OFC period. Consistent with previous reports,[19,30] the power proportion of theta rhythm was significantly enhanced in both the ACC and BLA of WT observer mice, temporally coinciding with vicarious freezing behavior. In contrast, we found that theta power changes were disrupted in both the ACC and BLA of SST-ARNT2 KO mice around the onset of freezing (Figure S10). Given that reciprocal communication within the ACC-BLA circuitry

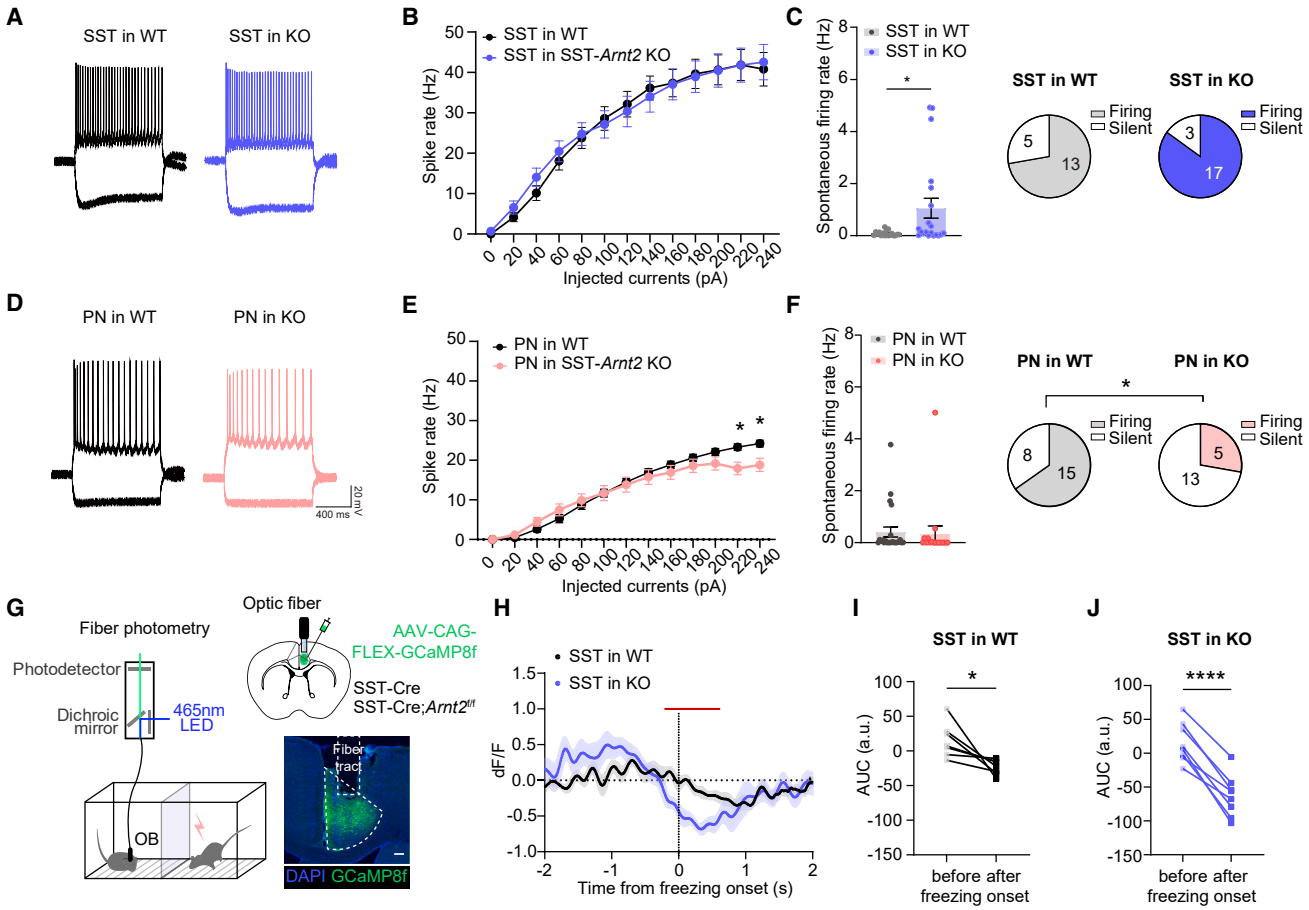

Figure 5. Enhanced spontaneous firing and altered *in vivo* Ca^{2+} dynamics in ARNT2-deficient SST neurons in the ACC

(A) Representative traces of changes in membrane potential and action potentials (APs) elicited by step-current injections in SST neurons from WT (*SST*$^{Cre/+}$; *Ai14*$^{F/+}$, left, black) and KO (*SST*$^{Cre/+}$;*Arnt2*$^{F/F}$;*Ai14*$^{F/+}$, right, blue) mice, respectively.

(B) Input-output (IO) curve of averaged frequency of AP firing at different step-current injections in SST neurons from WT (black) and SST-ARNT2 KO (blue) mice.

(C) The rate of spontaneous firing at −40 mV was significantly increased in ARNT2-deficient SST neurons (left), but the proportion of spontaneously firing SST cells was similar between WT (gray) and KO (blue) mice.

(D) Representative traces of changes in membrane potential and APs elicited by step-current injections in pyramidal neurons (PN) from WT (left, black) and SST-ARNT2 KO (right, pink), respectively.

(E) IO curve of average frequency of AP firing at different step-current injections in PNs from WT (black) and SST-ARNT2 KO (pink) mice. PNs demonstrated a substantially decreased number of APs at 220 and 240 pA current injections.

(F) No change in spontaneous firing rate in PNs from SST-ARNT2 KO mice (left). The proportion of spontaneously firing PNs was significantly lower in SST-ARNT2 KO (pink) than in WT mice (gray).

(G) Schematics of fiber photometry and the viral strategy to monitor Ca^{2+} dynamics in SST neurons in both WT (SST-Cre) and SST-ARNT2 KO (SST-Cre; *Arnt2*$^{F/F}$) mice during observational fear conditioning. AAV expressing Cre-dependent fluorescent Ca^{2+} indicator (AAV-CAG-FLEX-jGCaMP8f-WPRE) was injected into the right ACC of both WT and SST-ARNT2 KO mice. The representative image displays the fiber tract used for fiber photometry, with GCaMP8f signal in green and DAPI in blue. Scale bar, 200 μm.

(H) Average Ca^{2+} transients in SST neurons during vicarious freezing response were significantly lower in SST-ARNT2 KO mice than in WT mice (red dots, $p < 0.05$).

(I and J) Average Ca^{2+} activities before (−1 s to 0 s) and after (0 s to 1 s) the onset of freezing epochs. Both WT (I) and KO (J) mice showed a significant reduction in Ca^{2+} signals after the freezing onset.

All data are presented as mean ± SEM. *$p < 0.05$, **$p < 0.01$, ***$p < 0.001$ by two-way RM ANOVA followed by Šídák's post hoc test (B and E), unpaired t test with Welch's correction (C and F), cluster-based permutation test (H), and unpaired t test (I and J).

See also Figures S8 and S9; Table S1.

through theta oscillations is crucial for driving observational fear,[30] the aberrant activities of ARNT2-deficient SST neurons could impair ACC function, consequently leading to deficits in vicarious freezing behavior.

ARNT2-expressing SST neurons control emotional state discrimination

Empathy is an induction process that reflects an innate capacity to perceive and express sensitivity to the affective states of

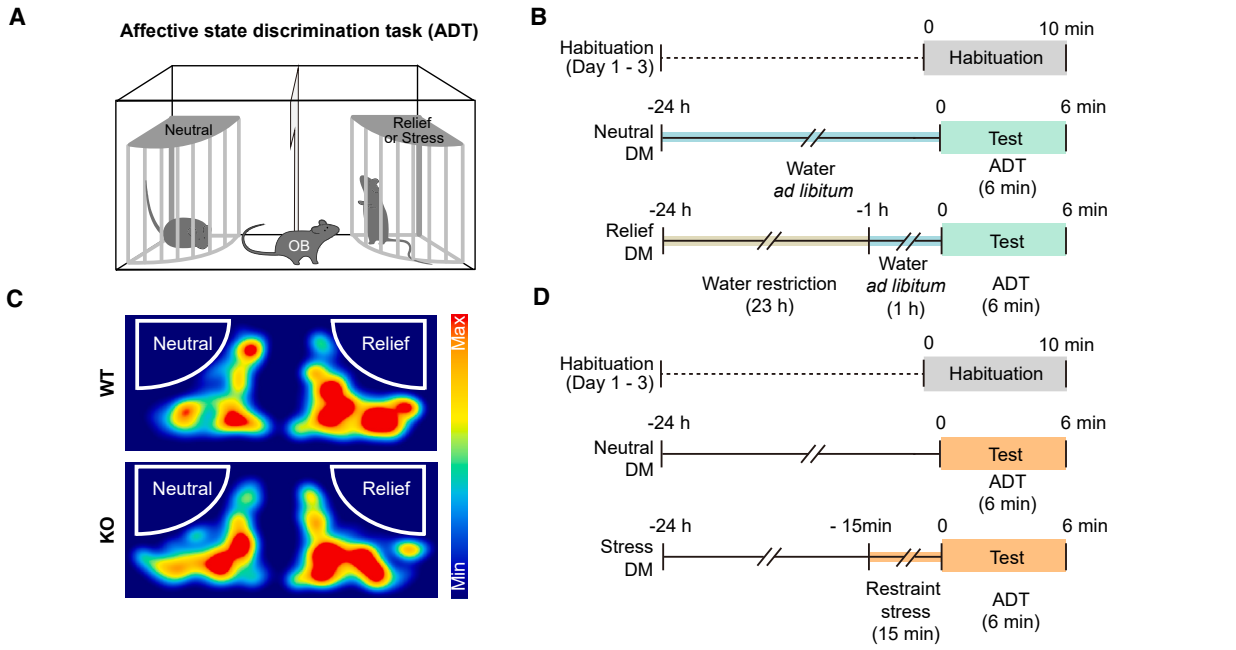

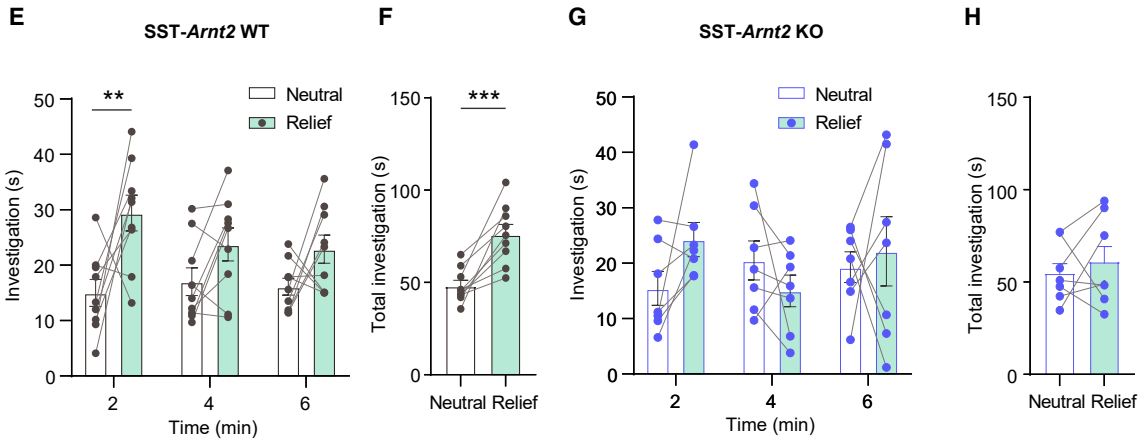

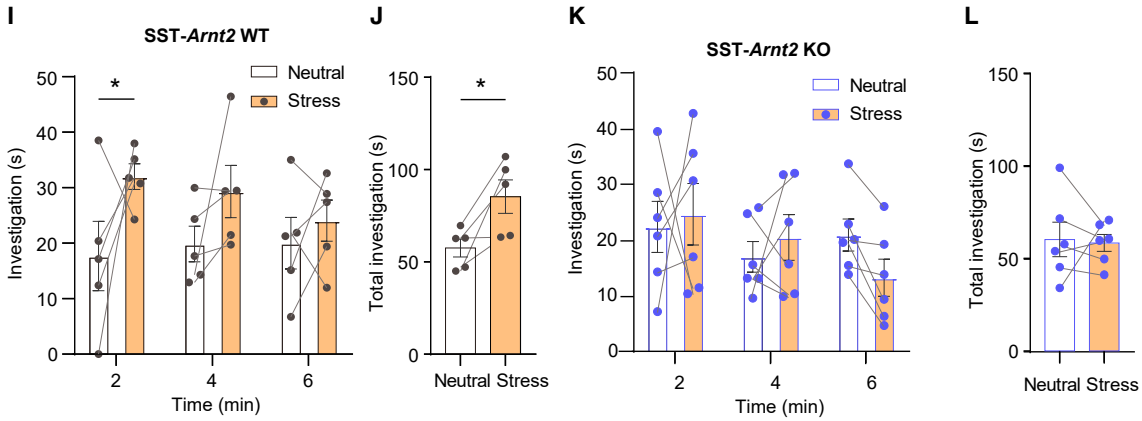

(legend on next page)

others. Witnessing how others feel and understanding their emotional states are fundamental for the development of empathy.[52,53] A previous genetic association study has demonstrated that the genetic polymorphism, rs4778599 SNP, located in intron 5 of *ARNT2*, is significantly associated with the ability to discern emotional expression in humans.[32] Intriguingly, SST interneurons in the prefrontal cortex, encompassing the prelimbic, infralimbic, and cingulate cortices, were found to play a crucial role in regulating emotion discrimination behavior in mice.[54,55] Thus, these findings raise an interesting question of whether ARNT2-expressing SST interneurons contribute to the ability to discern changes in the emotional state of others. To address this, we subjected SST-ARNT2 KO mice to an affective state discrimination task (ADT). In the social approach test of this paradigm, the observer is placed in a chamber with two demonstrators positioned at opposite ends, one of which has undergone an emotional state change (Figure 6A). Typically, observer mice exhibit a preference for exploring the arena containing the demonstrator with altered affective states.[54,56] To induce a relieved affective state, we subjected one demonstrator mouse to a 23-h water-deprivation period, followed by a 1-h period prior to testing during which water was provided (Figure 6B). The control demonstrator, positioned on the opposite side of the chamber, was allowed *ad libitum* access to water, serving as a neutral control. We observed that WT observer mice spent significantly more time exploring the emotionally altered demonstrator compared to the neutral one (Figures 6C, 6E, and 6F). In contrast, SST-ARNT2 KO mice failed to discriminate between the relieved demonstrator and the neutral control demonstrator (Figures 6C, 6G, and 6H).

Next, we investigated whether this impairment extended to negative affective states. We employed the same ADT but presented the observer with a demonstrator that underwent a mild stress protocol, consisting of 15 min of acute restraint immediately before the ADT (Figure 6D). The naive demonstrator on the other side of chamber served as a neutral control. WT observer mice displayed increased exploration toward the stressed demonstrators, spending significantly more time in the associated zone. This behavior was particularly evident during the first 2 min of observation (Figures 6I and 6J). In contrast, SST-ARNT2 KO mice again failed to discriminate between the stressed demonstrator and the neutral control demonstrator (Figures 6K and 6L). These findings, in conjunction with previous reports showing synchronous activity of SST neurons in observer mice during encounters with emotionally altered demonstrators,[54] suggest that ARNT2 plays a crucial role in the function of SST interneurons involved in emotional state discrimination.

DISCUSSION

Deficits or even lack of empathy are associated with various neuropsychiatric conditions,[57] yet either an animal model or an underlying circuit mechanism remains poorly understood. To address this, we employed an unbiased forward genetic mapping strategy in inbred mouse strains to pinpoint a specific gene crucial for observational fear. Our findings provide direct evidence that ARNT2, a transcription factor regulated by neuronal activity, plays a causal role in regulating observational fear by governing the activity of SST interneurons in the ACC. Moreover, the involvement of ARNT2-expressing SST inhibitory neurons in discriminating emotional states further corroborates its role in regulating empathic capacity in mice.

Our study showed that the markedly decreased observational fear response in AKR mice is likely caused by genetic variations that lead to dysfunction in the ACC rather than changes in sensory perception, anxiety levels, fear conditioning, or sociability behavior. By employing a combination of tools, including a recombinant congenic mouse, RNA-seq, and virus-mediated gene manipulation, we confirmed that genetic variations altering ARNT2 expression are responsible for the reduced vicarious freezing behavior in AKR mice. In particular, the ability of Arnt2

Figure 6. Emotional discrimination is impaired in SST-ARNT2 KO mice

(A) Diagram of affective state discrimination task (ADT).

(B) Outline of behavioral paradigm. Day 1 to day 3: observer (OB) and demonstrator (DM) mice are separately placed in a chamber or a wire cup for a 10-min period of free exploration (habituation). After the habituation is completed on day 3, demonstrator mice for the relief condition undergo a 23-h period of water deprivation. On the following day, they are given access to water for 1 h before the test. Day 4: the DM mouse is placed in the wire cup for the neutral and relief conditions, while the OB mouse is positioned at the center of the chamber. The duration of investigation is quantified during the 6-min testing period.

(C) Graphical representation of the amount of time spent by the WT and SST-ARNT2 KO observers in the testing chamber during positive ADT, with blue representing the shortest time and red indicating the longest time.

(D) Outline of stress paradigm (negative ADT) protocol. One demonstrator was subjected to the restraint stress test for 15 min immediately before the beginning of the ADT. The other neutral demonstrator waited undisturbed in the home cage. The duration of investigation is quantified during the 6-min testing period.

(E) Average investigation time in WT mice in positive ADT. WT mice showed an increased investigation time with the relieved demonstrator, as compared to the time spent with the neutral demonstrator during the initial 2 min of testing.

(F) The total investigation time of WT mice with the relieved demonstrator also increased during the 6-min period compared to that spent with the neutral demonstrator.

(G and H) Average investigation time in SST-ARNT2 KO mice in positive ADT. KO mice showed no difference in the investigation time between the neutral and relief demonstrators.

(I and J) Average investigation time in WT mice in negative ADT. WT mice showed an increased investigation time with the stressed demonstrator as compared to the time spent with the neutral demonstrator.

(K and L) Average investigation time in SST-ARNT2 KO mice. KO mice showed no significant difference in the investigation time between the neutral and stressed demonstrators.

All data are presented as mean ± SEM. $^{*}p < 0.05$, $^{**}p < 0.01$, $^{***}p < 0.001$ by two-way RM ANOVA followed by Bonferroni's post hoc test (E, G, I, and K) or two-tailed paired t test (F, H, J, and L).

See also Table S1.

knockdown to rescue observational fear suggests that the behavioral deficit in AKR mice is likely a consequence of elevated ARNT2 expression in the ACC. However, the precise mechanisms underlying the inability of shRNA-mediated Arnt2 gene knockdown in Oflq1 congenic mice to fully recapitulate the vicarious freezing behavior observed in WT B6N animals remain to be elucidated and warrant further investigation. Prior studies have demonstrated that large-effect QTLs often derive their robust effects from the cumulative contributions of multiple physically linked genes, each exerting smaller effect sizes.[58–60] Therefore, the possibility that additional genes within the *Oflq1* locus may modulate observational fear through distinct neurophysiological mechanisms cannot be excluded. In this context, we note that other DEGs within the *Oflq1* interval have well-established roles in brain functions, including neuronal energy metabolism (*Me3*), synaptic vesicle trafficking (*Sytl2*), myelin expression (*Fah*), and synaptic formation (*Cemip*).[61–64] These genes could potentially contribute to the overall observational fear response.

The temporal precision of activity-dependent gene transcription is essential for circuit modifications in response to changes in behavioral states.[65] In AKR mice, the abnormally elevated expression of the transcriptional repressor ARNT2 may inhibit the dynamics of activity-dependent gene expression in ACC neurons, which is crucial for the acquisition of observational fear behavior. We hypothesized that depleting ARNT2 using shRNA could reactivate these transcription networks, potentially enhancing behavioral responses in AKR mice. Surprisingly, overexpressing ARNT2 in B6N mice did not recapitulate the reduced observational fear response observed in AKR mice. We observed that reducing ARNT2 expression using the same shRNA in the B6N strain led to a similar reduction in observational fear. Moreover, neither CRISPR-mediated transcriptional activation nor SST neuron-specific overexpression of the *Arnt2* gene resulted in changes to observational fear response. These findings suggest that the genetic architecture governing ARNT2 expression in observational fear is highly complex, precluding a simple explanation. This observation aligns with a previous study demonstrating that ARNT2 plays dual roles in activity-dependent neuronal gene expression.[38,39] Under basal conditions, ARNT2 represses activity-dependent regulatory elements, maintaining low levels of inducible genes. Conversely, during high synaptic activity, ARNT2 recruits a neuron-specific transcription factor to enhance activity-dependent gene expression and alleviate transcriptional suppression.[38] The complex interplay between mouse strain-specific expressions of transcription factors, their developmental specification, and regulatory elements likely accounts for the differences in observational fear following ARNT2 depletion. Therefore, we propose that any perturbation in ARNT2 expression may disrupt activity-dependent transcription in ACC neurons, consequently reducing observational fear response. Nevertheless, because ARNT2 loss of function in SST neurons phenocopied behavioral deficits comparable to those observed in the AKR strain and B6N mice with shRNA-mediated knockdown, we surmise that the net physiological effect of aberrantly altered levels of ARNT2 expression is the disruption of the acquisition of observational fear.

Identification of the transcription factor ARNT2 in this study highlights the importance of activity-dependent gene regulation for the cellular function and circuit plasticity of SST interneurons in the ACC, specifically those involved in the regulation of observational fear. We have previously demonstrated that NRXN3, a presynaptic adhesion molecule, is selectively required for inhibitory synaptic transmission in SST interneurons and that ablation of NRXN3 in SST neurons in the ACC enhances observational fear.[66] Furthermore, optogenetic silencing of SST interneurons increases observational fear, whereas activation of SST neurons decreases the behavior, suggesting that SST interneurons in the ACC bidirectionally modulate the degree of vicarious freezing. Neocortical SST neurons exhibit a high rate of spontaneous firing[67,68] and their activity decreases during complex behaviors, which may facilitate synaptic plasticity and learning by enhancing excitatory transmission.[51,69,70] Consistently, our *in vivo* Ca^{2+} dynamics recording revealed that the reduced SST activity is directly associated with the observer's vicarious freezing behavior. Notably, the ablation of ARNT2 resulted in increased spontaneous firing in SST interneurons within the ACC. This elevated spontaneous firing may not only reduce local excitatory transmission between pyramidal cells but also diminish the excitatory drive onto SST neurons.[67,68] These changes may contribute to the aberrant activity patterns in ARNT2-deficient SST neurons during OFC. As a result, ACC dysfunction could impair theta oscillation synchrony within the ACC-BLA circuitry,[19,30] thereby impeding the induction of observational fear in SST-ARNT2 KO mice.

Mutations in specific components of activity-regulated signaling networks are known to contribute to psychiatric disorders, including intellectual disability, autism spectrum disorders, and schizophrenia.[39,71–74] Interestingly, genetic variants in *ARNT2* are associated with social cognition as well as susceptibility to autistic traits.[71,72] A particularly intriguing finding is that the *ARNT2* genetic polymorphism, rs4778599 SNP, exhibits a significant association with audiovisual emotion recognition in humans.[32] To functionally validate the role of ARNT2 in emotion recognition, we employed an affective state discrimination paradigm that approximates certain features of human emotion recognition tasks.[55,56,75] Since synchronous firing of SST interneurons is critical for affective state discrimination,[54] we posit that the aberrant activity of ARNT2-deficient SST neurons could compromise their precise regulatory influence on pyramidal cell activity within the ACC region of the prefrontal cortex, thereby impeding the affective capacity to recognize and respond appropriately to the emotional states of others. Collectively, our results provide a potential mechanism underlying genetic causality of *ARNT2* polymorphism for individual differences in emotion recognition. Furthermore, these findings suggest that the cellular and molecular mechanisms identified here are likely conserved between mice and humans. Therefore, it is plausible to propose that the recruitment of a distinct inhibitory microcircuit mediated by ARNT2-expressing SST neurons may represent an evolutionarily conserved and effective mechanism for modulating empathic capacity. This could be due to the specialized function of prefrontal SST neurons in integrating socially valenced information from multiple brain regions.[54,55,66]

ARNT2 is known to engage in protein-protein interactions with other bHLH-PAS transcription factors, particularly NPAS1, NPAS3, and NPAS4.[38,39,76] Our RNA-seq analysis revealed that among the 30 previously validated ARNT2-interacting genes,[38] only NPAS1 and NPAS3 showed differential expression between AKR and B6N mice in the naive state (Table S3). Interestingly, NPAS1 maintained elevated expression levels in AKR mice even in the post-OFC behavior state. NPAS1, a transcriptional repressor that requires ARNT2 for nuclear localization, plays a crucial role in modulating the number of SST neurons during cortical interneuron development.[76,77] This interaction provides valuable insights into the mechanisms governing cell-type-specific response.[76] Recent single-cell transcriptomic analyses have revealed that SST interneurons comprise eight major groups, each characterized by distinct molecular genetic profiles and specialized functional connectivity.[78,79] Future studies to uncover ARNT2-dependent transcriptional targets and their activity-dependent gene expression in distinct SST interneuron subtypes will provide insight into the ACC circuitry that orchestrates the regulation of empathic capacity.

In conclusion, we uncovered the selective and pivotal role of ARNT2 in the functional excitation of prefrontal SST interneurons that determines variability in empathic fear in mice. Given the evolutionary continuity of empathy from rodents to humans,[80,81] our findings provide valuable insights into the neurobiological basis of emotion recognition and affect sharing. Furthermore, this study contributes to a better understanding of the functional implications of *ARNT2* genetic variations in both healthy individuals and patients with psychiatric disorders characterized by empathy deficits.

Limitations of the study

Our results demonstrate that altered ARNT2 abundance causally contributes to observational fear deficits in the AKR mouse strain. However, the precise molecular mechanisms and genetic variations underlying the differential changes in observational fear resulting from ARNT2 depletion across mouse strains remain to be elucidated. Additionally, while we have identified aberrant activity patterns in ARNT2-deficient SST neurons during the onset of vicarious freezing, the functional connections between these *in vivo* Ca^{2+} dynamics and electrophysiological properties need further clarification, especially regarding the spontaneous firing of SST neurons and the altered excitability of pyramidal neurons in the ACC.

STAR★METHODS

Detailed methods are provided in the online version of this paper and include the following:

SUPPLEMENTAL INFORMATION

Supplemental information can be found online at https://doi.org/10.1016/j.celrep.2024.114659.

ACKNOWLEDGMENTS

This work was supported by the Institute for Basic Science (IBS), Center for Cognition and Sociality (IBS-R001-D2 to S.K.); the Basic Science Research Program through the National Research Foundation of Korea (NRF) funded by the Ministry of Science and ICT (RS-2023-00253215 to S.C.); the Bio & Medical Technology Development Program of the NRF funded by the Korean government (NRF-2022M3E5E8017701 to S.C.); the Global Learning & Academic research institution for Master's·PhD students, and Postdocs (G-LAMP) Program of the NRF funded by the Ministry of Education (RS-2023-00301850); and the Korea Brain Research Institute (KBRI) basic research program through KBRI funded by the Ministry of Science and ICT and Future Planning (grants 23-BR-03-04 to S.C., J.K., and S.K.).

AUTHOR CONTRIBUTIONS

Conceptualization, H.-S.S. and S. Keum; methodology, S. Chae and S. Keum; investigation, J.C., S.J., Jieun Kim, D.S., A.K., S. Kim, J.Y.K., E.Y., S. Choi, H.L., and Y.C.J.; writing – original draft, J.C., S.J., S. Chae, and S. Keum; writing – review and editing, J.C., S.J., D.S., S. Chae, and S. Keum; funding acquisition, S. Chae, Jeongyeon Kim, and S. Keum; supervision, S. Chae and S. Keum.

DECLARATION OF INTERESTS

The authors declare no competing interests.

Received: January 16, 2024
Revised: July 1, 2024
Accepted: August 5, 2024
Published: August 24, 2024

REFERENCES

1. Bernhardt, B.C., and Singer, T. (2012). The neural basis of empathy. Annu. Rev. Neurosci. *35*, 1–23. https://doi.org/10.1146/annurev-neuro-062111-150536.
2. de Waal, F.B.M. (2008). Putting the altruism back into altruism: the evolution of empathy. Annu. Rev. Psychol. *59*, 279–300. https://doi.org/10.1146/annurev.psych.59.103006.093625.
3. Rodrigues, S.M., Saslow, L.R., Garcia, N., John, O.P., and Keltner, D. (2009). Oxytocin receptor genetic variation relates to empathy and stress reactivity in humans. Proc. Natl. Acad. Sci. USA *106*, 21437–21441. https://doi.org/10.1073/pnas.0909579106.
4. Knafo, A., Zahn-Waxler, C., Davidov, M., Van Hulle, C., Robinson, J.L., and Rhee, S.H. (2009). Empathy in early childhood: genetic, environmental,

and affective contributions. Ann. N. Y. Acad. Sci. *1167*, 103–114. https://doi.org/10.1111/j.1749-6632.2009.04540.x.

5. Warrier, V., Grasby, K.L., Uzefovsky, F., Toro, R., Smith, P., Chakrabarti, B., Khadake, J., Mawbey-Adamson, E., Litterman, N., Hottenga, J.J., et al. (2018). Genome-wide meta-analysis of cognitive empathy: heritability, and correlates with sex, neuropsychiatric conditions and cognition. Mol. Psychiatry *23*, 1402–1409. https://doi.org/10.1038/mp.2017.122.
6. Baron-Cohen, S., and Wheelwright, S. (2004). The empathy quotient: an investigation of adults with Asperger syndrome or high functioning autism, and normal sex differences. J. Autism Dev. Disord. *34*, 163–175. https://doi.org/10.1023/b:jadd.0000022607.19833.00.
7. Bora, E., Gökçen, S., and Veznedaroglu, B. (2008). Empathic abilities in people with schizophrenia. Psychiatry Res. *160*, 23–29. https://doi.org/10.1016/j.psychres.2007.05.017.
8. Thoma, P., Zalewski, I., von Reventlow, H.G., Norra, C., Juckel, G., and Daum, I. (2011). Cognitive and affective empathy in depression linked to executive control. Psychiatry Res. *189*, 373–378. https://doi.org/10.1016/j.psychres.2011.07.030.
9. Decety, J., Chen, C., Harenski, C., and Kiehl, K.A. (2013). An fMRI study of affective perspective taking in individuals with psychopathy: imagining another in pain does not evoke empathy. Front. Hum. Neurosci. *7*, 489. https://doi.org/10.3389/fnhum.2013.00489.
10. Avinun, R., Israel, S., Shalev, I., Gritsenko, I., Bornstein, G., Ebstein, R.P., and Knafo, A. (2011). AVPR1A variant associated with preschoolers' lower altruistic behavior. PLoS One *6*, e25274. https://doi.org/10.1371/journal.pone.0025274.
11. Bachner-Melman, R., Gritsenko, I., Nemanov, L., Zohar, A.H., Dina, C., and Ebstein, R.P. (2005). Dopaminergic polymorphisms associated with self-report measures of human altruism: a fresh phenotype for the dopamine D4 receptor. Mol. Psychiatry *10*, 333–335. https://doi.org/10.1038/sj.mp.4001635.
12. Keum, S., and Shin, H.S. (2019). Genetic factors associated with empathy in humans and mice. Neuropharmacology *159*, 107514. https://doi.org/10.1016/j.neuropharm.2019.01.029.
13. Murphy, D.G.M., Daly, E., Schmitz, N., Toal, F., Murphy, K., Curran, S., Erlandsson, K., Eersels, J., Kerwin, R., Ell, P., and Travis, M. (2006). Cortical serotonin 5-HT2A receptor binding and social communication in adults with Asperger's syndrome: an in vivo SPECT study. Am. J. Psychiatry *163*, 934–936. https://doi.org/10.1176/ajp.2006.163.5.934.
14. Pearce, E., Wlodarski, R., Machin, A., and Dunbar, R.I.M. (2017). Variation in the beta-endorphin, oxytocin, and dopamine receptor genes is associated with different dimensions of human sociality. Proc. Natl. Acad. Sci. USA *114*, 5300–5305. https://doi.org/10.1073/pnas.1700712114.
15. Rodrigues, S.M., Saslowc, L.R., Garciac, N., John, O.P., and Keltner, D. (2009). Oxytocin receptor genetic variation relates to empathy and stress reactivity in humans. Proc. Natl. Acad. Sci. USA *106*, 21437–21441.
16. Warrier, V., Toro, R., Chakrabarti, B., iPSYCH-Broad autism group; Børglum, A.D., Grove, J., 23andMe Research Team; Hinds, D.A., Bourgeron, T., and Baron-Cohen, S. (2018). Genome-wide analyses of self-reported empathy: correlations with autism, schizophrenia, and anorexia nervosa. Transl. Psychiatry *8*, 35. https://doi.org/10.1038/s41398-017-0082-6.
17. Warrier, V., and Baron-Cohen, S. (2018). Genetic contribution to 'theory of mind' in adolescence. Sci. Rep. *8*, 3465. https://doi.org/10.1038/s41598-018-21737-8.
18. Woodbury-Smith, M.R., Paterson, A.D., Szatmari, P., and Scherer, S.W. (2020). Genome-wide association study of emotional empathy in children. Sci. Rep. *10*, 7469. https://doi.org/10.1038/s41598-020-62693-6.
19. Jeon, D., Kim, S., Chetana, M., Jo, D., Ruley, H.E., Lin, S.Y., Rabah, D., Kinet, J.P., and Shin, H.S. (2010). Observational fear learning involves affective pain system and Cav1.2 Ca2+ channels in. Nat. Neurosci. *13*, 482–488. https://doi.org/10.1038/nn.2504.
20. Olsson, A., and Phelps, E.A. (2007). Social learning of fear. Nat. Neurosci. *10*, 1095–1102. https://doi.org/10.1038/nn1968.
21. Keum, S., and Shin, H.S. (2016). Rodent models for studying empathy. Neurobiol. Learn. Mem. *135*, 22–26. https://doi.org/10.1016/j.nlm.2016.07.022.
22. Sivaselvachandran, S., Acland, E.L., Abdallah, S., and Martin, L.J. (2018). Behavioral and mechanistic insight into rodent empathy. Neurosci. Biobehav. Rev. *91*, 130–137. https://doi.org/10.1016/j.neubiorev.2016.06.007.
23. Panksepp, J.B., and Lahvis, G.P. (2011). Rodent empathy and affective neuroscience. Neurosci. Biobehav. Rev. *35*, 1864–1875. https://doi.org/10.1016/j.neubiorev.2011.05.013.
24. Keum, S., and Shin, H.S. (2019). Neural Basis of Observational Fear Learning: A Potential Model of Affective Empathy. Neuron *104*, 78–86. https://doi.org/10.1016/j.neuron.2019.09.013.
25. Singer, T., Seymour, B., O'Doherty, J., Kaube, H., Dolan, R.J., and Frith, C. (2004). Empathy for Pain Involves the Affective but not Sensory Components of Pain. Science *303*, 1157–1162.
26. Allsop, S.A., Wichmann, R., Mills, F., Burgos-Robles, A., Chang, C.J., Felix-Ortiz, A.C., Vienne, A., Beyeler, A., Izadmehr, E.M., Glober, G., et al. (2018). Corticoamygdala Transfer of Socially Derived Information Gates Observational Learning. Cell *173*, 1329–1342.e18. https://doi.org/10.1016/j.cell.2018.04.004.
27. Carrillo, M., Han, Y., Migliorati, F., Liu, M., Gazzola, V., and Keysers, C. (2019). Emotional Mirror Neurons in the Rat's Anterior Cingulate Cortex. Curr. Biol. *29*, 1301–1312.e6. https://doi.org/10.1016/j.cub.2019.03.024.
28. Huang, Z., Chung, M., Tao, K., Watarai, A., Wang, M.Y., Ito, H., and Okuyama, T. (2023). Ventromedial prefrontal neurons represent self-states shaped by vicarious fear in male mice. Nat. Commun. *14*, 3458. https://doi.org/10.1038/s41467-023-39081-5.
29. Terranova, J.I., Yokose, J., Osanai, H., Marks, W.D., Yamamoto, J., Ogawa, S.K., and Kitamura, T. (2022). Hippocampal-amygdala memory circuits govern experience-dependent observational fear. Neuron *110*, 1416–1431.e13. https://doi.org/10.1016/j.neuron.2022.01.019.
30. Kim, S.W., Kim, M., Baek, J., Latchoumane, C.F., Gangadharan, G., Yoon, Y., Kim, D.S., Lee, J.H., and Shin, H.S. (2023). Hemispherically lateralized rhythmic oscillations in the cingulate-amygdala circuit drive affective empathy in mice. Neuron *111*, 418–429.e4. https://doi.org/10.1016/j.neuron.2022.11.001.
31. Keum, S., Park, J., Kim, A., Park, J., Kim, K.K., Jeong, J., and Shin, H.S. (2016). Variability in empathic fear response among 11 inbred strains of mice. Genes Brain Behav. *15*, 231–242. https://doi.org/10.1111/gbb.12278.
32. Hovey, D., Henningsson, S., Cortes, D.S., Bänziger, T., Zettergren, A., Melke, J., Fischer, H., Laukka, P., and Westberg, L. (2018). Emotion recognition associated with polymorphism in oxytocinergic pathway gene ARNT2. Soc. Cogn. Affect. Neurosci. *13*, 173–181. https://doi.org/10.1093/scan/nsx141.
33. Brown, R.E., and Wong, A.A. (2007). The influence of visual ability on learning and memory performance in 13 strains of mice. Learn. Mem. *14*, 134–144. https://doi.org/10.1101/lm.473907.
34. O'Leary, T.P., Savoie, V., and Brown, R.E. (2011). Learning, memory and search strategies of inbred mouse strains with different visual abilities in the Barnes maze. Behav. Brain Res. *216*, 531–542. https://doi.org/10.1016/j.bbr.2010.08.030.
35. Wong, A.A., and Brown, R.E. (2006). Visual detection, pattern discrimination and visual acuity in 14 strains of mice. Genes Brain Behav. *5*, 389–403. https://doi.org/10.1111/j.1601-183X.2005.00173.x.
36. Zheng, Q.Y., Johnson, K.R., and Erway, L.C. (1999). Assessment of hearing in 80 inbred strains of mice by ABR threshold analyses. Hear. Res. *130*, 94–107. https://doi.org/10.1016/s0378-5955(99)00003-9.
37. Yates, A.D., Achuthan, P., Akanni, W., Allen, J., Allen, J., Alvarez-Jarreta, J., Amode, M.R., Armean, I.M., Azov, A.G., Bennett, R., et al. (2020). Ensembl 2020. Nucleic Acids Res. *48*, D682–D688. https://doi.org/10.1093/nar/gkz966.

38. Sharma, N., Pollina, E.A., Nagy, M.A., Yap, E.L., DiBiase, F.A., Hrvatin, S., Hu, L., Lin, C., and Greenberg, M.E. (2019). ARNT2 Tunes Activity-Dependent Gene Expression through NCoR2-Mediated Repression and NPAS4-Mediated Activation. Neuron *102*, 390–406.e9. https://doi.org/10.1016/j.neuron.2019.02.007.

39. Pollina, E.A., Gilliam, D.T., Landau, A.T., Lin, C., Pajarillo, N., Davis, C.P., Harmin, D.A., Yap, E.L., Vogel, I.R., Griffith, E.C., et al. (2023). A NPAS4-NuA4 complex couples synaptic activity to DNA repair. Nature *614*, 732–741. https://doi.org/10.1038/s41586-023-05711-7.

40. Konermann, S., Brigham, M.D., Trevino, A.E., Joung, J., Abudayyeh, O.O., Barcena, C., Hsu, P.D., Habib, N., Gootenberg, J.S., Nishimasu, H., et al. (2015). Genome-scale transcriptional activation by an engineered CRISPR-Cas9 complex. Nature *517*, 583–588. https://doi.org/10.1038/nature14136.

41. Liao, H.K., Hatanaka, F., Araoka, T., Reddy, P., Wu, M.Z., Sui, Y., Yamauchi, T., Sakurai, M., O'Keefe, D.D., Núñez-Delicado, E., et al. (2017). In Vivo Target Gene Activation via CRISPR/Cas9-Mediated Trans-epigenetic Modulation. Cell *171*, 1495–1507.e15. https://doi.org/10.1016/j.cell.2017.10.025.

42. Hosoya, T., Oda, Y., Takahashi, S., Morita, M., Kawauchi, S., Ema, M., Yamamoto, M., and Fujii-Kuriyama, Y. (2001). Defective development of secretory neurones in the hypothalamus of Arnt2-knockout mice. Gene Cell. *6*, 361–374. https://doi.org/10.1046/j.1365-2443.2001.00421.x.

43. Keith, B., Adelman, D.M., and Simon, M.C. (2001). Targeted mutation of the murine arylhydrocarbon receptor nuclear translocator 2 (Arnt2) gene reveals partial redundancy with Arnt. Proc. Natl. Acad. Sci. USA *98*, 6692–6697. https://doi.org/10.1073/pnas.121494298.

44. Saunders, A., Macosko, E.Z., Wysoker, A., Goldman, M., Krienen, F.M., de Rivera, H., Bien, E., Baum, M., Bortolin, L., Wang, S., et al. (2018). Molecular Diversity and Specializations among the Cells of the Adult Mouse Brain. Cell *174*, 1015–1030.e16. https://doi.org/10.1016/j.cell.2018.07.028.

45. Tremblay, R., Lee, S., and Rudy, B. (2016). GABAergic Interneurons in the Neocortex: From Cellular Properties to Circuits. Neuron *91*, 260–292. https://doi.org/10.1016/j.neuron.2016.06.033.

46. Atsak, P., Orre, M., Bakker, P., Cerliani, L., Roozendaal, B., Gazzola, V., Moita, M., and Keysers, C. (2011). Experience modulates vicarious freezing in rats: a model for empathy. PLoS One *6*, e21855. https://doi.org/10.1371/journal.pone.0021855.

47. Sakaguchi, T., Iwasaki, S., Okada, M., Okamoto, K., and Ikegaya, Y. (2018). Ethanol facilitates socially evoked memory recall in mice by recruiting pain-sensitive anterior cingulate cortical neurons. Nat. Commun. *9*, 3526. https://doi.org/10.1038/s41467-018-05894-y.

48. Sanders, J., Mayford, M., and Jeste, D. (2013). Empathic fear responses in mice are triggered by recognition of a shared experience. PLoS One *8*, e74609. https://doi.org/10.1371/journal.pone.0074609.

49. Keysers, C., Knapska, E., Moita, M.A., and Gazzola, V. (2022). Emotional contagion and prosocial behavior in rodents. Trends Cogn. Sci. *26*, 688–706. https://doi.org/10.1016/j.tics.2022.05.005.

50. Gentet, L.J., Kremer, Y., Taniguchi, H., Huang, Z.J., Staiger, J.F., and Petersen, C.C.H. (2012). Unique functional properties of somatostatin-expressing GABAergic neurons in mouse barrel cortex. Nat. Neurosci. *15*, 607–612. https://doi.org/10.1038/nn.3051.

51. Urban-Ciecko, J., and Barth, A.L. (2016). Somatostatin-expressing neurons in cortical networks. Nat. Rev. Neurosci. *17*, 401–409. https://doi.org/10.1038/nrn.2016.53.

52. Decety, J., Norman, G.J., Berntson, G.G., and Cacioppo, J.T. (2012). A neurobehavioral evolutionary perspective on the mechanisms underlying empathy. Prog. Neurobiol. *98*, 38–48. https://doi.org/10.1016/j.pneurobio.2012.05.001.

53. de Waal, F.B.M., and Preston, S.D. (2017). Mammalian empathy: behavioural manifestations and neural basis. Nat. Rev. Neurosci. *18*, 498–509. https://doi.org/10.1038/nrn.2017.72.

54. Scheggia, D., Managò, F., Maltese, F., Bruni, S., Nigro, M., Dautan, D., Latuske, P., Contarini, G., Gomez-Gonzalo, M., Requie, L.M., et al. (2020). Somatostatin interneurons in the prefrontal cortex control affective state discrimination in mice. Nat. Neurosci. *23*, 47–60. https://doi.org/10.1038/s41593-019-0551-8.

55. Dautan, D., Monai, A., Maltese, F., Chang, X., Molent, C., Mauro, D., Galbusera, A., Vecchia, D., Antonelli, F., Benedetti, A., et al. (2024). Cortico-cortical transfer of socially derived information gates emotion recognition. Nat. Neurosci. *27*, 1318–1332. https://doi.org/10.1038/s41593-024-01647-x.

56. Ferretti, V., Maltese, F., Contarini, G., Nigro, M., Bonavia, A., Huang, H., Gigliucci, V., Morelli, G., Scheggia, D., Managò, F., et al. (2019). Oxytocin Signaling in the Central Amygdala Modulates Emotion Discrimination in Mice. Curr. Biol. *29*, 1938–1953.e6. https://doi.org/10.1016/j.cub.2019.04.070.

57. Decety, J., and Moriguchi, Y. (2007). The empathic brain and its dysfunction in psychiatric populations: implications for intervention across different clinical conditions. Biopsychosoc. Med. *1*, 22. https://doi.org/10.1186/1751-0759-1-22.

58. Flint, J. (2011). Mapping quantitative traits and strategies to find quantitative trait genes. Methods *53*, 163–174. https://doi.org/10.1016/j.ymeth.2010.07.007.

59. Keum, S., Lee, H.K., Chu, P.L., Kan, M.J., Huang, M.N., Gallione, C.J., Gunn, M.D., Lo, D.C., and Marchuk, D.A. (2013). Natural genetic variation of integrin alpha L (Itgal) modulates ischemic brain injury in stroke. PLoS Genet. *9*, e1003807. https://doi.org/10.1371/journal.pgen.1003807.

60. Legare, M.E., Bartlett, F.S., and Frankel, W.N. (2000). A major effect QTL determined by multiple genes in epileptic EL mice. Genome Res. *10*, 42–48.

61. Kuroda, T.S., Fukuda, M., Ariga, H., and Mikoshiba, K. (2002). The Slp homology domain of synaptotagmin-like proteins 1-4 and Slac2 functions as a novel Rab27A binding domain. J. Biol. Chem. *277*, 9212–9218. https://doi.org/10.1074/jbc.M112414200.

62. Moore, M.E., Koenig, A.E., Hillgartner, M.A., Otap, C.C., Barnby, E., and MacGregor, G.G. (2017). Abnormal social behavior in mice with tyrosinemia type I is associated with an increase of myelin in the cerebral cortex. Metab. Brain Dis. *32*, 1829–1841. https://doi.org/10.1007/s11011-017-0071-8.

63. Motori, E., Atanassov, I., Kochan, S.M.V., Folz-Donahue, K., Sakthivelu, V., Giavalisco, P., Toni, N., Puyal, J., and Larsson, N.G. (2020). Neuronal metabolic rewiring promotes resilience to neurodegeneration caused by mitochondrial dysfunction. Sci. Adv. *6*, eaba8271. https://doi.org/10.1126/sciadv.aba8271.

64. Yoshino, Y., Shimazawa, M., Nakamura, S., Inoue, S., Yoshida, H., Shimoda, M., Okada, Y., and Hara, H. (2018). Targeted deletion of HYBID (hyaluronan binding protein involved in hyaluronan depolymerization/KIAA1199/CEMIP) decreases dendritic spine density in the dentate gyrus through hyaluronan accumulation. Biochem. Biophys. Res. Commun. *503*, 1934–1940. https://doi.org/10.1016/j.bbrc.2018.07.138.

65. Yap, E.L., and Greenberg, M.E. (2018). Activity-Regulated Transcription: Bridging the Gap between Neural Activity and Behavior. Neuron *100*, 330–348. https://doi.org/10.1016/j.neuron.2018.10.013.

66. Keum, S., Kim, A., Shin, J.J., Kim, J.H., Park, J., and Shin, H.S. (2018). A Missense Variant at the Nrxn3 Locus Enhances Empathy Fear in the Mouse. Neuron *98*, 588–601.e5. https://doi.org/10.1016/j.neuron.2018.03.041.

67. Kanigowski, D., Bogaj, K., Barth, A.L., and Urban-Ciecko, J. (2023). Somatostatin-expressing interneurons modulate neocortical network through GABAb receptors in a synapse-specific manner. Sci. Rep. *13*, 8780. https://doi.org/10.1038/s41598-023-35890-2.

68. Urban-Ciecko, J., Fanselow, E.E., and Barth, A.L. (2015). Neocortical somatostatin neurons reversibly silence excitatory transmission via GABAb receptors. Curr. Biol. *25*, 722–731. https://doi.org/10.1016/j.cub.2015.01.035.

69. Kvitsiani, D., Ranade, S., Hangya, B., Taniguchi, H., Huang, J.Z., and Kepecs, A. (2013). Distinct behavioural and network correlates of two interneuron types in prefrontal cortex. Nature *498*, 363–366. https://doi.org/10.1038/nature12176.

70. Lovett-Barron, M., Kaifosh, P., Kheirbek, M.A., Danielson, N., Zaremba, J.D., Reardon, T.R., Turi, G.F., Hen, R., Zemelman, B.V., and Losonczy, A. (2014). Dendritic inhibition in the hippocampus supports fear learning. Science *343*, 857–863. https://doi.org/10.1126/science.1247485.

71. Chakrabarti, B., Dudbridge, F., Kent, L., Wheelwright, S., Hill-Cawthorne, G., Allison, C., Banerjee-Basu, S., and Baron-Cohen, S. (2009). Genes related to sex steroids, neural growth, and social-emotional behavior are associated with autistic traits, empathy, and Asperger syndrome. Autism Res. *2*, 157–177. https://doi.org/10.1002/aur.80.

72. Di Napoli, A., Warrier, V., Baron-Cohen, S., and Chakrabarti, B. (2015). Genetic variant rs17225178 in the ARNT2 gene is associated with Asperger Syndrome. Mol. Autism. *6*, 9. https://doi.org/10.1186/s13229-015-0009-0.

73. Ebert, D.H., and Greenberg, M.E. (2013). Activity-dependent neuronal signalling and autism spectrum disorder. Nature *493*, 327–337. https://doi.org/10.1038/nature11860.

74. De Rubeis, S., He, X., Goldberg, A.P., Poultney, C.S., Samocha, K., Cicek, A.E., Kou, Y., Liu, L., Fromer, M., Walker, S., et al. (2014). Synaptic, transcriptional and chromatin genes disrupted in autism. Nature *515*, 209–215. https://doi.org/10.1038/nature13772.

75. Henry, J.D., von Hippel, W., Molenberghs, P., Lee, T., and Sachdev, P.S. (2016). Clinical assessment of social cognitive function in neurological disorders. Nat. Rev. Neurol. *12*, 28–39. https://doi.org/10.1038/nrneurol.2015.229.

76. Stanco, A., Pla, R., Vogt, D., Chen, Y., Mandal, S., Walker, J., Hunt, R.F., Lindtner, S., Erdman, C.A., Pieper, A.A., et al. (2014). NPAS1 represses the generation of specific subtypes of cortical interneurons. Neuron *84*, 940–953. https://doi.org/10.1016/j.neuron.2014.10.040.

77. Teh, C.H.L., Lam, K.K.Y., Loh, C.C., Loo, J.M., Yan, T., and Lim, T.M. (2006). Neuronal PAS domain protein 1 is a transcriptional repressor and requires arylhydrocarbon nuclear translocator for its nuclear localization. J. Biol. Chem. *281*, 34617–34629. https://doi.org/10.1074/jbc.M604409200.

78. Wu, S.J., Sevier, E., Dwivedi, D., Saldi, G.A., Hairston, A., Yu, S., Abbott, L., Choi, D.H., Sherer, M., Qiu, Y., et al. (2023). Cortical somatostatin interneuron subtypes form cell-type-specific circuits. Neuron *111*, 2675–2692.e9. https://doi.org/10.1016/j.neuron.2023.05.032.

79. Gouwens, N.W., Sorensen, S.A., Baftizadeh, F., Budzillo, A., Lee, B.R., Jarsky, T., Alfiler, L., Baker, K., Barkan, E., Berry, K., et al. (2020). Integrated Morphoelectric and Transcriptomic Classification of Cortical GABAergic Cells. Cell *183*, 935–953.e19. https://doi.org/10.1016/j.cell.2020.09.057.

80. Panksepp, J., and Panksepp, J.B. (2013). Toward a cross-species understanding of empathy. Trends Neurosci. *36*, 489–496. https://doi.org/10.1016/j.tins.2013.04.009.

81. Paradiso, E., Gazzola, V., and Keysers, C. (2021). Neural mechanisms necessary for empathy-related phenomena across species. Curr. Opin. Neurobiol. *68*, 107–115. https://doi.org/10.1016/j.conb.2021.02.005.

82. Gonzalez-Liencres, C., Juckel, G., Tas, C., Friebe, A., and Brüne, M. (2014). Emotional contagion in mice: the role of familiarity. Behav. Brain Res. *263*, 16–21. https://doi.org/10.1016/j.bbr.2014.01.020.

83. Park, J., Ha, S., Shin, H.S., and Jeong, J. (2022). Experience of a hierarchical relationship between a pair of mice specifically influences their affective empathy toward each other. Genes Brain Behav. *21*, e12810. https://doi.org/10.1111/gbb.12810.

84. Hong, E.H., and Choi, J.S. (2018). Observational threat conditioning is induced by circa-strike activity burst but not freezing and requires visual attention. Behav. Brain Res. *353*, 161–167. https://doi.org/10.1016/j.bbr.2018.06.034.

85. Broman, K.W., Wu, H., Sen, S., and Churchill, G.A. (2003). R/qtl: QTL mapping in experimental crosses. Bioinformatics *19*, 889–890. https://doi.org/10.1093/bioinformatics/btg112.

86. Smith, R., Sheppard, K., DiPetrillo, K., and Churchill, G. (2009). Quantitative trait locus analysis using J/qtl. Methods Mol. Biol. *573*, 175–188. https://doi.org/10.1007/978-1-60761-247-6_10.

87. Cox, A., Ackert-Bicknell, C.L., Dumont, B.L., Ding, Y., Bell, J.T., Brockmann, G.A., Wergedal, J.E., Bult, C., Paigen, B., Flint, J., et al. (2009). A new standard genetic map for the laboratory mouse. Genetics *182*, 1335–1344. https://doi.org/10.1534/genetics.109.105486.

88. Anders, S., Pyl, P.T., and Huber, W. (2015). HTSeq–a Python framework to work with high-throughput sequencing data. Bioinformatics *31*, 166–169. https://doi.org/10.1093/bioinformatics/btu638.

89. Robinson, M.D., and Oshlack, A. (2010). A scaling normalization method for differential expression analysis of RNA-seq data. Genome Biol. *11*, R25. https://doi.org/10.1186/gb-2010-11-3-r25.

90. Chae, S., Ahn, B.Y., Byun, K., Cho, Y.M., Yu, M.H., Lee, B., Hwang, D., and Park, K.S. (2013). A systems approach for decoding mitochondrial retrograde signaling pathways. Sci. Signal. *6*, rs4. https://doi.org/10.1126/scisignal.2003266.

91. Fortenbery, G.W., Sarathy, B., Carraway, K.R., and Mansfield, K.D. (2018). Hypoxic stabilization of mRNA is HIF-independent but requires mtROS. Cell. Mol. Biol. Lett. *23*, 48. https://doi.org/10.1186/s11658-018-0112-2.

92. Maris, E., and Oostenveld, R. (2007). Nonparametric statistical testing of EEG- and MEG-data. J. Neurosci. Methods *164*, 177–190. https://doi.org/10.1016/j.jneumeth.2007.03.024.

STAR★METHODS

KEY RESOURCES TABLE

REAGENT or RESOURCE	SOURCE	IDENTIFIER
Antibodies		
ARNT2 antibody	Santa Cruz	Cat# sc-393683 (B11); RRID:AB_2783034
ARNT2 antibody	ELK Biotechnology	Cat# ES8125; RRID: N/A
CRE Recombinase antibody	Millipore	Cat# MAB3120; RRID:AB_2085748
Tubulin Beta 3 (TUBB3) antibody	BioLegend	Cat# 801201; RRID:AB_2313773
Goat anti-Mouse IgG (H + L) Highly Cross-Adsorbed Secondary Antibody, Alexa Fluor™ 594	Thermo Fisher Scientific	Cat# A-11032; RRID:AB_2534091
Alexa Fluor 488 donkey anti-mouse	Jackson ImmunoResearch Labs	Cat# 715-545-150; RRID:AB_2340846
Alexa Fluor 488 donkey anti-Rabbit	Jackson ImmunoResearch Labs	Cat# 711-545-152; RRID:AB_2313584
Bacterial and virus strains		
AAV DJ/8-CAG-FLEX-jGCaMP8f-WPRE	IBS virus facility	N/A
AAV DJ/8-CamKIIa-Cre-GFP	IBS virus facility	N/A
AAV DJ/8-CamKIIa-GFP	IBS virus facility	N/A
AAV9.EF1a.fDIO.Cre.WPRE	UNC GTC vector	N/A
AAV5.EF1a.fDIO.eYFP.WPRE	UNC GTC vector	N/A
AAV-U6-Arnt2 shRNA-CMV-mCherry	IBS virus facility	N/A
AAV-U6-Scramble shRNA-CMV-mCherry	IBS virus facility	N/A
Chemicals, peptides, and recombinant proteins		
SouthernBiotech DAPI Fluoromount-G	SouthernBiotech	Cat#0100-20
Critical commercial assays		
Mouse Low Density Linkage SNP Panels	Illumina	GT-18-121
TruSeq Stranded mRNA (NovaSeq 6000 System)	Illumina	Cat# 20020594
SensiFAST™ SYBR® No-ROX Kit	Bioline	Cat# BIO-98050
Deposited data		
RNA-seq data	This paper	GEO database: GSE248193
Experimental models: Organisms/strains		
Mouse: C57BL/6NJ inbred strain	Jackson Laboratory	JAX: 005304, RRID:IMSR_JAX:005304
Mouse: AKR/J inbred strain	Jackson Laboratory	JAX: 000648, RRID:IMSR_JAX:000648
Mouse: B6J.Vglut2-IRES-Cre: B6J.129S6(FVB)-Slc17a6tm2(cre)Lowl/MwarJ	Jackson Laboratory	JAX: 028863, RRID:IMSR_JAX:028863
Mouse: B6J.Vgat-IRES-Cre: *Slc32a1tm2(cre)Lowl*/J	Jackson Laboratory	JAX: 016962, RRID:IMSR_JAX:016962
Mouse: B6J.PV-IRES-Cre: B6J.129P2-*Pvalbtm1(cre)Arbr*/J	Jackson Laboratory	JAX: 008069, RRID:IMSR_JAX:008069
Mouse: Ai14 Rosa26LSL-tdT: B6.Cg-*Gt(ROSA)26Sortm14(CAG-tdTomato)Hze*/J	Jackson Laboratory	JAX: 007914, RRID:IMSR_JAX:007914
Mouse: B6J.VIP-IRES-Cre: B6J.*Viptm1(cre)Zjh*/J	Jackson Laboratory	JAX: 010908, RRID:IMSR_JAX:010908
Mouse: B6J.SST-IRES-Cre: Ssttm2.1(cre)Zjh/J	Jackson Laboratory	JAX: 013044, RRID:IMSR_JAX:013044
Mouse: B6J.SST-IRES-Flp: *Ssttm3.1(flpo)Zjh*/J	Jackson Laboratory	JAX: 028579, RRID:IMSR_JAX:028579
Mouse: B6J.NDNF-IRES-Cre: *Ndnftm1.1(cre)Rudy/J*	Jackson Laboratory	JAX: 030757, RRID:IMSR_JAX:030757
Mouse: B6J. ARNT2 conditional knockout (KO)	This paper	N/A
Oligonucleotides		
ARNT2 floxed genotyping primer: forward 5′- AGATGGGGAGAATGGTTGCTTAC -3′	This paper	N/A

(*Continued on next page*)

Continued

REAGENT or RESOURCE	SOURCE	IDENTIFIER
ARNT2 floxed genotyping primer: reverse 5′- GGATTGATAGATGAGCAGCAAGAA -3′	This paper	N/A
Arnt2 shRNA sequence: CGCTATTATCATGCCATAGAT	This paper	N/A
Control shRNA sequence: CCTAAGGTTAAGTCGCCCTCG	VectorBuilder	N/A
Arnt2 qPCR primer: forward 5′- GAAGACG CTGATGTCGGACAAG-3′	This paper See Table S4 for qPCR primers	N/A
Arnt2 qPCR primer: reverse 5′- CAGAGTT GTGCCGTGACAGGAA -3′	This paper See Table S4 for qPCR primers	N/A
Recombinant DNA		
pAAV-CAG-FLEX-jGCaMP8f-WPRE	Addgene	Plasmid #162382
pAAV-CamKIIa-Cre-GFP	IBS virus facility	N/A
pAAV-CamKIIa-GFP	IBS virus facility	N/A
pAAV-U6-Arnt2 shRNA-CMV-mCherry	VectorBuilder	N/A
pAAV-U6-scramble shRNA-CMV-mCherry	VectorBuilder	N/A
pAAV-U6-Arnt2 gRNA-Ef1a-MS2/P65/HSF1	VectorBuilder	N/A
pAAV-CMV-dSaCAS9/VP64	VectorBuilder	N/A
Software and algorithms		
FreezeFrame	Coulbourn Instruments	Cat# ACT-100A
Graphpad Prism 10	GraphPad Software	https://www.graphpad.com/
Zen lite	Zeiss	http://www.zwiss.com
R/qtl	R/qtl package	http://www.rqtl.org
pCLAMP 11.2	Axon Instruments	N/A
Doric Neuroscience studio	Doric lenses inc.	https://neuro.doriclenses.com/
MATLAB R2020a	Mathworks	mathworks.com/
Fiber photometry analysis (FPA)	https://github.com/leomol/FPA	N/A
Chronux software package	http://chronux.org	N/A
Other		
Optic fibers 400 μm core, 0.50 NA, ZF 1.25, DFL	Newdoon	FOC-C-B-400-1.25-0.50-1.5
RHD 32-Channel Recording Headstages	Intan technologies	Part #C3324
Open Ephys acquisition board	Open Ephys	N/A

RESOURCE AVAILABILITY

Lead contact

Further information and requests for resources and reagents should be directed to and will be fulfilled by the lead contact, Sehoon Keum (sdukeum@ibs.re.kr).

Materials availability

A mouse line generated in this study is available from the lead contact with a completed Materials Transfer Agreement.

Data and code availability

- RNA-Seq data has been deposited into the Gene Expression Omnibus (GEO) database with accession ID: GSE248193.
- This study does not report original code. Fiber photometry acquisition and analysis code were based upon the fiber photometry analysis (FPA) toolbox (https://github.com/leomol/FPA).
- Any additional information required to reanalyze the data reported in this study is available from the lead contact upon request.

EXPERIMENTAL MODEL AND SUBJECT DETAILS

Mice

All inbred mice (AKR/J and C57BL/6NJ), *SST*$^{tm2.1(cre)Zjh/J}$ (SST-Cre), *Pvalb*$^{tm1(cre)Arbr}$ (PV-Cre), *Vip*$^{tm1(cre)Zjh}$ (VIP-Cre), *Ndnf*$^{tm1.1(cre)Rudy/J}$ (NDNF-Cre), *Slc17a6*$^{tm2(cre)Lowl/J}$(Vglut2-ires-Cre), and Gt(ROSA)26Sor$^{tm14(CAG-tdTomato)Hze}$ (*Ai14* Rosa26$^{LSL-tdT}$) strains were obtained from The Jackson Laboratory (Bar Harbor, USA) and bred in-house for experiments. All animals were housed in groups of 2–5 per cage. The cages were maintained under a 12/12-h light/dark cycle at a temperature of 23°C–25°C. Food and water were available *ad libitum*. Male littermates were randomly assigned to either the experimental or control group. Behavioral tests were conducted on visibly healthy male mice (i.e., no skin irritation, agility, and no developmental malformation of eyes or teeth) aged 10–14 weeks.). To maximize the statistical power of our forward genetic mapping and identify all potential genetic determinants associated with environmental factors environmental factors, such as familiarity or social hierarchy,[19,82,83] we employed only male mice in this study. Electrophysiological slice experiments involving whole-cell patch clamp recordings were performed on mice aged 5–19 weeks. All experiments were approved by the Institutional Animal Care and Use Committee of the Institute for Basic Science (IBS).

METHOD DETAILS

Behaviors

All behavioral tests were conducted between 2 and 7p.m. during the light cycle. Additionally, the Day-2 contextual memory test was carried out at a similar time of day as conditioning. Mice were placed in their respective home cages in the behavioral test room approximately an hour before the tests. We used naive mice, with no prior experience of any behaviors, only once for each of the behavioral assays. Each behavioral test was performed as mice became available from breeding (from at least 3 different litters), and not in any particular order by strain or mutant line. Sample sizes were estimated based on previous studies with similar experimental designs.[31,66]

Observational fear conditioning

Male mice, aged 10–14 weeks (both observer and demonstrator), were individually placed in chambers partitioned by a porous, transparent Plexiglas divider in the middle. After a 5-min habituation period, a 2-s foot shock (1 mA) was delivered every 10 s for 4 min to the demonstrator mouse.[19,31] To assess contextual memory, the observer mice were returned to the chamber 24-h after training for 4 min. In all experiments, the observer and demonstrator mice were neither siblings nor cagemates. The behavior of the mice was recorded using the Freezeframe software (Coulbourn Instruments, USA) and primarily analyzed with the FreezeView software (Coulbourn Instruments, USA), with manual validation by experimenters. Motionless bouts lasting more than 1 s were considered as freezing. In the experience-dependent observational fear paradigm,[29,46,47] the observer mouse underwent contextual fear conditioning (FC) 24 h prior to OFC task. FC occurred in a distinct context (dim yellow light, black striped wall, lavender scent). The observer was placed into the fear conditioning chamber for a 3 min habituation period, received a 1mA, 1sec foot shock, and remained in the fear conditioning chamber for a total of 2 min. Additionally, observers' gazing behavior was analyzed.[84] The gazing behavior was defined as the head orienting itself toward a demonstrator, and the duration of this behavior was measured manually.

Affective state discrimination

Experimental mice (observers and demonstrators) were habituated for 10 min each day, starting from three days before the testing day,[54] in a chamber (31.5 × 17 × 19 cm) that we had custom-made. The testing chamber was divided into two zones by an opaque separator (12 × 19 cm), which included passageways allowing observer mice to pass through. At both ends of the chamber, there were funnel-shaped wire cups, with one demonstrator mouse for each affective condition placed inside each wire cup (bottom diameter 10 cm, 31 cm in height). The separator between the two wire cups was sufficient to block the line of sight between the demonstrators. To prevent bias based on olfactory cues, all chambers and accessories were cleaned with super hypochlorous water and 70% ethanol every time the subjects were changed. The testing chamber was placed within a custom-made soundproof cubicle with a dim light (8 lx).

Observer and demonstrator mice were matched by age and sex. Observer mice were habituated inside the testing chamber without a demonstrator present. If an observer mouse spent more than 75 percentage of its time on one side of the testing chamber for more than two out of three habituation days, it was excluded from the affective state discrimination test. Demonstrators were habituated separately, without the observer, inside the same cage under the wire cups. The presentation of neutral versus relief demonstrators was counterbalanced on the two sides of the testing arena. Neutral demonstrators were allowed to remain undisturbed in their home cages with unrestricted access to water. All neutral demonstrators were group-housed, separately from the cages of relieved demonstrators. Relieved demonstrators underwent a 23-h period of water deprivation and provided access to water 1 h prior to the affective state discrimination test.

Digital cameras (Logitech, c922 pro) were positioned above the cages to capture the recordings, which were manually analyzed by experimenters. The investigation behaviors involved the observer mouse either sniffing within 1 inch of the wire cup or directing its head toward the demonstrator while using its forepaws to interact. Representative images in Figure 6 were plotted using EthoVision XT software (Noldus, Netherlands).

Pavlovian fear conditioning

On training day, mice were placed in the fear conditioning chamber (Coulbourn Instruments, USA). After a 3 min exploration period, 3 foot shocks (0.7mA/1 s) separated by 1 min intervals were delivered to the mice. The mice remained in training chamber for another 60 s before being returned to home cages. Freezing behavior of the mice was recorded and analyzed with FreezeView software as described above. Motionless bouts lasting more than 2 s were considered as freezing.

Open field

Exploratory activity in a novel environment was assessed during a 30-min test in an open field box. Each mouse was placed on the periphery of the field, and the paths of the freely exploring animals were recorded for 30 min using a video camera. The center time was calculated as the percentage of time spent in the central 18% of the field, and the distance traveled was measured in total centimeters covered. The open-field box, measuring 50 × 45 × 40 cm, was made of gray plastic, and the center was defined as a square area (20 × 20 cm). The videos were analyzed using EthoVision XT software (Noldus, Netherlands).

Elevated plus maze

Mice were given a single 5-min trial on the plus-maze, which consisted of two white open arms (25 × 8 × 0 cm), two black enclosed arms (25 × 8 × 20 cm), and a central platform (8 × 8 × 8 cm) arranged in the shape of a cross. The maze was elevated 50 cm above the floor. Each mouse was individually placed on the center section, facing one of the closed arms. The total time spent in each arm or the center, and the total number of entries into each arm, were analyzed by video monitoring over a 5-min period. The percentage of time spent in the open arms was calculated using the formula: 100 × (time spent on the open arms/(time in the open arms + time in the closed arms)).

Three-chamber sociability test

Sociability was assessed in an automated three-chambered social approach apparatus. The test animals were placed in a Plexiglas arena (60 × 40 × 22 cm) with opaque-white walls, divided into a center chamber and two side chambers. Each group of mice was naive to this task and all other tasks, and had not been exposed to the arena prior to testing. Retractable doors built into the two dividing walls allowed access to the side chambers. The subject mouse was acclimated to the apparatus with a 10-min habituation session in all three empty chambers before sociability testing. The subject was then briefly confined to the center chamber while a novel object (an inverted steel-wire cage) was placed in one side chamber and a novel mouse (stranger 1) inside an identical inverted wire cage was placed in the other side chamber. Once both wire cages were positioned, the two side doors were lifted, and the subject mouse was allowed access to all three chambers for 10 min. The novel unfamiliar strangers used were age- and sex-matched mice of the same strain as the subject mice. The movement of the test mouse was video-recorded, and the amount of time spent in each chamber was analyzed using the EthoVision XT software (Noldus, Netherlands).

QTL mapping

Linkage mapping was performed on informative SNP markers and total vicarious freezing time (sec) of 190 F2 recombinants using the scan one function in the R/qtl package (http://www.rqtl.org).[85] Threshold levels of significance were established using at least 1,000 permutations of the respective dataset. Genome-wide scans were plotted using the J/QTL mapping program.[86] Results were expressed as logarithm of the odds (LOD) scores. Significant ($p = 0.05$) threshold was established empirically for each phenotypic trait by 1,000 permutation tests using all informative markers. The LOD score threshold level, set at a confidence level of .05 (generally accepted for statistical significance) was 3.31. The percentage of total trait variance attributable to each locus was determined using the Fit-QTL function provided within the J/QTL software.

Genotyping

Single nucleotide polymorphism (SNP) genotyping was performed using the Golden Gate genome-wide mouse 377 SNP panel (Illumina, CA, USA). Genomic positions of genetic markers (NCBI GRCm29/mm39) were retrieved from the UCSC genome browser (http://www.genome.ucsc.edu/) and converted to cM by using the mouse map converter (http://cgd.jax.org/mousemapconverter/).[87] The distal boundary of the critical interval (7.7 Mbp) of B6N.AKR-*Oflq1* was determined by locations of maximal break points for the genotyped markers. The *Oflq1* critical interval was homozygous for B6N alleles at Chr7: 83.5 Mbp (rs36537392, Chr7: 83,541,244 bp) and at Chr7: 91.2 Mbp (D7Mit301, Chr7: 9,123,119-91,233,239 bp).

Generation of congenic mice

AKR and B6N strains were intercrossed to generate F1 mice, which were then backcrossed to B6N for ten generations. The presence of the AKR-derived observational fear learning locus (*Oflq1*) on chromosome 7 in the offspring of each generation was detected using the AKR-B6N polymorphic microsatellite marker (D7Mit62, located at Chr7: 84,290,094-84,290,240 bp). Additionally, SNPs (rs8247788, rs36537392, and rs31840595) and microsatellite markers (D7Mit163, D7Mit301, and D7Mit96) flanking the *Oflq1* locus were used for fine-mapping of the B6N.AKR-*Oflq1* congenic mice.

Bulk RNA sequencing

Total RNA was obtained from ACC tissues of male AKR and B6N mice under naive or 90-min post-observational fear conditions. At the time of tissue extraction, the bilateral ACC tissue punches from three animals were pooled to create four independent biological replicates for the naive group (12 mice in total for each strain) and three for the post-observational fear group (9 mice in total for each

strain). The samples were then flash-frozen on dry ice. The integrity of the total RNA in each sample was analyzed using a 2100 Bioanalyzer (Agilent Technologies, Santa Clara, CA, USA). The RNA integrity values for all the samples were greater than 8. Poly (A) mRNA was isolated from the total RNA and subsequent fragmentation was performed using the TruSeq Stranded mRNA LT Sample Prep Kit (Illumina, San Diego, CA, USA), according to the manufacturer's instructions. The adaptor-ligated libraries were sequenced using Illumina NovaSeq 6000 (Macrogen, Inc., Seoul, South Korea). From the resulting read sequences for each sample, adapter sequences (TruSeq universal and indexed adapters) were removed using cutadapt software (version 2.7; https://cutadapt.readthedocs.io/en/stable/). The remaining reads were then aligned to the *Mus musculus* reference genome (GRCm38) using STAR software (version 2.7.9) with default parameters. After the alignment, we counted the number of reads mapped to the gene features (GTF file of GRCm38.91) using HTSeq.[88] Read counts for the samples in each condition were normalized using the TMM (trimmed mean of M-value) normalization of the edgeR package.[89] The raw data were deposited into the Gene Expression Omnibus database with accession ID GSE248193.

Identification of differentially expressed genes (DEGs)

The number of reads for the gene features counted by HTseq was converted to $\log_2$-values after adding one (pseudo count) to the read counts. To identify the DEGs, hypothesis testing was performed.[90] For each gene, a *t*-statistic value was calculated using Student's *t*-test for the comparison of AKR versus B6N. An empirical distribution of the T-statistic value for the null hypothesis (i.e., the genes are not differentially expressed) was then estimated by performing all possible combinations of random permutations of the samples. The *p*-values from Student's *t*-test for each gene were computed using a two-tailed test with an empirical null distribution. The DEGs were identified as genes with *p*-values <0.05 and absolute $\log_2$ fold changes larger than the cutoff (0.429; 1.35 fold change), which corresponded to the 2.5th and 97.5th percentiles of the null distribution. Ensembl IDs, Entrez IDs, symbols, descriptions, *p*-values, and $\log_2$ fold changes of the 1,779 DEGs are documented in Table S2.

Quantitative RT-PCR

The mRNA levels of genes that are up- or down-regulated in AKR mice (*Arnt2*, *Fah*, *Me3*, *Sytl2*, *Cemip*, *Prss23*) were evaluated by real-time PCR. RNA were extracted from the ACC of both B6N and AKR mice using Nucleozol (Macherey-Nagel, Cat No. 740404.200, Dueren, Germany) according to manufacturer's instruction. cDNA was synthesized with Superscript cDNA Premix Kit II (GeNetBio) and were subjected to 40-cycle real-time PCR using SensiFAST SYBR No-ROX Kit (Bioline, Cat No. BIO-98050, Memphis, TN, USA) and a CFX Duet Real-Time PCR System (Bio-Rad, Hercules, CA, USA). The *Gapdh* cycle threshold (Ct) value was used for normalization. The fold changes of genes from the ACC of AKR mice was calculated relative to that of B6N mice. The primer sequences are provided in Table S3.

DNA construct for shRNA-mediated knockdown

To deplete ARNT2 in ACC neurons for behavioral experiments, control Scramble shRNA (CCTAAGGTTAAGTCGCCCTCG) and *Arnt2* shRNA (CGCTATTATCATGCCATAGAT) were cloned downstream of the U6 promoter, and mCherry was driven off the CMV promoter (VectorBuilder, USA). All AAV backbones (AAV-U6-shRNA-CMV-mCherry) were generated using standard cloning and molecular biology techniques. AAVs (serotype DJ/8) were prepared by the Institute for Basic Science Virus facility.

Generation of *Arnt2* conditional KO mice

Given the absence of sequence variations at the *Arnt2* gene locus between the C57BL/6NJ (B6N) and B6J strains (https://mpd.jax.org/genotypes), and all Cre-driver mice of B6J background obtained from The Jackson Laboratory, we utilized CRISPR/Cas9 technology to generate the conditional allele of the *Arnt2* gene (NCBI Reference Sequence: NM_007488.3; Ensembl: ENSMUSG00000015709). The $Arnt2^{F/F}$ conditional knockout (KO) mice were designed by flanking exon2 (ENSMUSE00000530046) and exon3 (ENSMUSE00000530045) of the *Arnt2*-201 transcript (ENSMUST00000085077.5) which contains a 163 bp coding sequence, with one pair of *loxP* sites. The verification of deletion of exon2-3 was confirmed by Sanger DNA sequencing after cloning PCR product from positive F0 generation $Arnt2^{F/+}$ mice. Positive F0 mice were bred with B6J mice for two generations before intercrossing heterozygous $Arnt2^{F/+}$ mice to produce homozygous $Arnt2^{F/F}$ animals. All mice employed in Figures 4, 5, and 6 were of the B6J strain genetic background. Mice with conditional deletion of $Arnt2^{F/F}$ in SST-expressing neurons were obtained by first crossing $Arnt2^{F/F}$ females with SST-Cre male mice. Then, $SST^{Cre/+}$; $Arnt2^{F/+}$ males were crossed with $Arnt2^{F/F}$ female mice to obtain homozygous conditional KO mice ($SST^{Cre/+}$; $Arnt2^{F/F}$). SST-ARNT2 KO mice, along with their respective WT littermates ($Arnt2^{F/F}$), were used in the experiments. Mouse genotyping was determined by PCR of mouse tail genomic DNA. The genotype of the *Arnt2* gene was amplified using standard PCR conditions (94°C for 2min, 94°C for 30 s, 60°C for 30 s, 72°C for 30 s, 30 cycles). The genotype primers amplifies a 365-bp PCR product from the *LoxP* floxed allele and a 297-bp PCR product from the WT allele.

Western blot

Mice were anesthetized with isoflurane and decapitated for brain extraction. The ACC was isolated on ice and acutely homogenized with ice-cold brain homogenization buffer (0.32M sucrose, 10mM HEPES, 2mM EDTA, 2mM EGTA, protease inhibitors, and phosphatase inhibitors, pH 7.4). Proteins were resolved on 10% Tris-Glycine gels and transferred to nitrocellulose. Membranes were incubated overnight in the following primary antibodies[91]: ARNT2 (Santa Cruz Cat#sc-393683 (B11), 1:50) and beta-TUBULIN3

(BioLegend, MMS-435P). HRP-conjugated secondary antibody signals were captured (ChemiDoc XRS+, BioRad, USA) and immunoblot signals were quantified using ImageJ software.

Histology

Mice underwent perfusion and fixation for examination of virus infection topography and position of optic fiber. Mice were intraperitoneally injected with about 0.8mL 2% Avertin in saline solution. When they were fully anesthetized, they were transcardially infused with saline, followed by 4% paraformaldehyde (PFA) in 0.1M phosphate-buffered saline (PBS). The harvested brains were post-fixed in 4% PFA (kept at a temperature below 4°C) overnight. Subsequently, the fixed brains were sectioned into 30μm coronal slices using a vibratome (Leica VT 1200S). For antigen retrieval, slice samples were incubated in 1mL of 1% NaOH and 1% H_2O_2 in 0.1 M PBS for 10 min. Following this, the slices were incubated in 1mL of 0.3% glycine in 0.1 M PBS for 10 min. Slice samples were then blocked in a 5% serum solution composed of a 3:2 ratio of normal donkey serum (NDS) and normal goat serum (NGS) with 0.25% Triton X-(Sigma, T8787) in 100 mM Phosphate Buffer (PB) (NaH_2PO_4 and $NaPO_4$, pH 7.4) for 1hour at 25°C. After 2× washes in 100 mM PB, the slices were incubated in a primary antibody solution (0.25% Triton X-100, 5% NDS/NGS, in PB, along with rabbit polyclonal anti-ARNT2 (1:100, ELK Biotechnology, ES8125) and mouse monoclonal anti-CRE) for 17 h at 4°C on a rotating platform. The slices were then washed three times in PB and incubated for 4 h at 4°C in a secondary antibody solution (0.25% Triton X-100, 5% NDS/NGS, in PB, along with Alexa Fluor 488 donkey anti-rabbit (1:500, Jackson ImmunoResearch Labs) and Alexa Fluor 594 goat anti-mouse (1:500, Invitrogen)) before being mounted on a glass slide using the DAPI Fluoromount-G antifade mounting medium (SouthernBiotech).

Virus injection and *in vivo* surgery

Adult mice were first put in a gas chamber (Vapormatic Ltd) filled with a mixture of isoflurane (4%) and oxygen (at 2L/min), and anesthetized with 8 mg/mL ketamine (16% by volume) and xylazine (2.8% by volume) in saline solution intraperitoneally injected (0.015 mL/g). Anesthetized mice were head-fixed on a stereotaxic equipment (Kopf Instruments). A heating pad ensured maintenance of core body temperature at 36°C. Antiseptics and lidocaine were applied before making incision on skin. Single or multiple cranial openings were made with dental drills, then a volume of about 0.5μL virus solution was injected using pressure (Picospritzer III, Parker Hannifin Corp.) into the right ACC (AP/MD/DV, 1.0/0.3/1.5 mm). The injection glass pipette was then slowly removed after 10 min for diffusion. For fiber photometry, a 400 μm diameter mono fiber optic cannula (Newdoon, FOC-C-B-400-1.25-0.50-1.5, China) was targeted to the same position as that used for the virus injection, dental cement was applied to cover the skull, and was allowed to harden for 10 min. Behavioral experiments were performed at least 3 weeks post-surgery. Cell-type-specific expression of virus was achieved using the following AAV vectors: pAAV-CAG-FLEX-jGCaMP8f-WPRE (Addgene), pAAV-CamKIIα-Cre-GFP (Addgene), pAAV-CamKIIα-GFP (IBS virus facility), AAV.EF1a.fDIO.Cre.WPRE (UNC GTC vector core), and AAV.EF1a.fDIO.eYFP.WPRE (UNC GTC vector core). All serotype DJ/8 AAV were prepared by the Institute for Basic Science Virus facility (https://www.ibs.re.kr/virusfacility/).

Fiber photometry recording

Fiber photometry was used to record cell-type-specific expression of GCaMP8f calcium transients from SST neurons in the right ACC of both SST-Cre and SST-Cre; *Arnt2*$^{F/F}$ mice. Animals were handled and habituated to the optic fiber in their home cages for 10 min a day over a span of 3 days. A fiber photometry system from Doric Lenses was used, which included two excitation LEDs (465 nm and 405 nm) controlled by an LED driver and a fiber photometry console. The entire system was operated through Doric Neuroscience Studio software (Doric Lenses Inc.). The LEDs were modulated at frequencies of 208.616 Hz (405 nm) and 572.205 Hz (465 nm), and the resulting signal was demodulated using lock-in amplification. The excitation light was delivered to the animal through a low-autofluorescence mono fiber optic patch cord (Doric, MFP_FCM-MF1.25_LAF). The detected signal was collected using a photoreceiver. The GCaMP8f signal was acquired at a rate of 12.0 kSps and subsequently subjected to downsampling to 100 Hz. Data was exported to MATLAB R2021a (Mathworks) for offline analysis using the fiber photometry analysis (FPA) toolbox (https://github.com/leomol/FPA) and custom-written scripts in MATLAB. To identify the difference in Ca^{2+} signal levels between the two groups, a cluster-based permutation test was employed.[92] Baseline correction was performed by modeling an exponential decay of the full trace data filtered at 4 Hz. Motion artifacts were subsequently corrected by subtracting a reference signal from the data after applying a polynomial fit. Data were normalized as df/f = (f-f0)/f1, where f0 represents the median and f1 the median absolute deviation (MAD) calculated from all data points.

Local field potential (LFP) recordings and analysis

Tungsten electrodes (0.003″ diameter; A-M systems) were implanted stereotaxically into ACC (AP/MD/DV, 1.0/0.35/-1.65 mm) and BLA (AP/MD/DV, −1.4/3.15/-4.7 mm). A reference electrode was implanted on the cerebellum cortex. Dental acrylic cement was applied to secure the electrodes to the skull. Following at least one week of post-surgical recovery, mice underwent habituation to the recording environment and tethered cables for two consecutive days within the recording chamber. Electrophysiological recordings were obtained using RHD 32-channel recording headstages (Intan Technologies) and the electrical signals were amplified and digitized at a sampling rate of 1 kHz using a digital acquisition system (Open Ephys). Video monitoring was synchronized with the acquisition board using pulse generator (Pulse Pal). *In vivo* LFPs were analyzed using the MATLAB and Chronux software package

(http://chronux.org).[30] LFP signals were reduced in sampling rate to 1 kHz. To remove very low-frequency fluctuations from the recorded LFP, a local detrending procedure (function locdetrend.m in Chronux) was applied. The signals were then bandpass filtered between 1 and 40 Hz for detailed analysis. To eliminate artifacts from the demonstrator's electrical shock, data segments from −500 ms before to 500 ms after the shock (total 3 s for every shock epoch including the 2 s-shock period) were excluded from analysis. The estimated power was normalized against the total power at each time point. For each subject, the normalized power was weighted by the duration of freezing and averaged across freezing periods. Changes related to freezing were examined by converting the weighted average power at each frequency into z-scores, using the period from −1.5 to −1 s before the onset of freezing as a baseline.

Slice patch-clamp recording

Fully anesthetized animals were decapitated and coronal slices of ACC (300μm) were prepared in oxygenated (95% O_2, 5% CO_2), cold sucrose cutting solution, and recovered in a recording chamber perfused with oxygenated artificial cerebral spinal fluid (ACSF) recording solution at RT. APs and spontaneous firings were measured with an internal solution filling patch pipette (4–7 MΩ). Signal recordings were performed using a Multiclamp 700B amplifier and Digidata 1550A (Axon Instruments, USA), and the acquired data were analyzed using pCLAMP 11.2 (Axon Instruments, USA). SST+ neurons were recognized through the presence of tdTomato fluorescent expression. Action potentials (APs) were triggered by a 1 s long, with an incremental increase of 20 pA in current clamp (CC) mode. Spontaneous firing was recorded with the membrane potential held at −40 mV in voltage clamp mode. The action potential properties were analyzed during the first action potential, which occurred when a 120pA current was injected. Sucrose cutting solution (in mM): sucrose, 212.5; D-glucose, 10; $NaHCO_3$, 26; KCl, 3; $MgCl_2$, 5; $CaCl_2$, 0.1; NaH_2PO_4,1.25; pH 7.3, and 300 mOsm. ACSF recording solution (in mM) was NaCl, 130; KCl, 3.5; $NaHCO_3$, 20.17; $MgCl_2$, 1.5; $CaCl_2$, 1.5; NaH_2PO_4, 1.25; D-glucose, 10; pH 7.2, 310 mOsm. Internal solution (in mM) was K-gluconate, 120; NaCl, 2; KCl, 20; Glucose, 10; HEPES, 20; EGTA, 0.5; NA-ATP, 2; Na-GTP, 0.5; KHCO3, 20; pH 7.3, 295 mOsm.

QUANTIFICATION AND STATISTICAL ANALYSIS

All data presented indicate means ± SEM. Statistical analyses were performed using Prism 10 (GraphPad Software, USA). Normality was assessed using Shapiro-Wilk tests. When the normality test failed, subject group analysis of non-parametric data was done with Kruskal-Wallis statistics followed by Dunn's multiple comparison test. No statistical methods were used to predetermine sample size. Variance in normally distributed datasets was analyzed with one-way or two-way analysis of variance (ANOVA) and Šídák's *post-hoc* tests. Single variable comparisons were made with two-tailed Student's *t*-tests. For *ex vivo* patch recording, statistical analysis of cumulative probabilities was tested by a Kolmogorov-Smirnov test from: http://www.physics.csbsju.edu/stats/KS-test.n.plot_form.html. Significance levels are indicated as follows. $^{*}p < 0.05$; $^{**}p < 0.01$; $^{***}p < 0.001$.